

# Resistance and Wake Prediction for Early Stage Ship Design

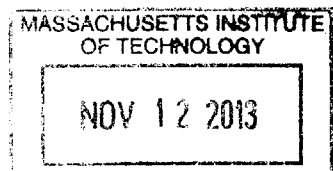
by  
Brian Johnson

B.S., University of Massachusetts Lowell, 2008

Submitted to the Department of Mechanical Engineering  
in partial fulfillment of the requirements for the degree of  
Master of Naval Architecture and Marine Engineering  
at the

MASSACHUSETTS INSTITUTE OF TECHNOLOGY  
September 2013

ARCHIVED



LIBRARIES

© Massachusetts Institute of Technology 2013. All rights reserved.

Author .....  
Department of Mechanical Engineering  
August 20, 2013

Certified by .....  
Chrysostomos Chrysostomidis  
Doherty Professor of Ocean Science and Engineering  
Thesis Supervisor

Certified by .....  
Stefano Brizzolara  
Research Scientist and Lecturer, Mechanical Engineering  
Thesis Supervisor

Certified by .....  
Douglas Read  
Associate Professor Maine Maritime Academy  
Thesis Supervisor

Accepted by .....  
David E. Hardt  
Graduate Officer, Department of Mechanical Engineering



# **Resistance and Wake Prediction for Early Stage Ship Design**

by

Brian Johnson

Submitted to the Department of Mechanical Engineering  
on August 20, 2013, in partial fulfillment of the  
requirements for the degree of  
Master of Naval Architecture and Marine Engineering

## **Abstract**

Before the detailed design of a new vessel a designer would like to explore the design space to identify an appropriate starting point for the concept design. The base design needs to be done at the preliminary design level with codes that execute fast to completely explore the design space. The intent of this thesis is to produce a preliminary design tool that will allow the designer to predict the total resistance and propeller wake for use in an optimization program, having total propulsive efficiency as an objective function. There exist design tools to predict the total resistance and propeller wake, but none that provide adequate computational times for the preliminary design stage. The tool developed uses a potential flow solution coupled with an integral boundary layer solver to predict the viscous resistance and propeller wake. The wave drag is calculated using a modified linear theory, thus eliminating the need to run fully three-dimensional free surface CFD codes. The tool developed is validated against published Series 60 test data.

Thesis Supervisor: Chryssostomos Chryssostomidis  
Title: Doherty Professor of Ocean Science and Engineering

Thesis Supervisor: Stefano Brizzolara  
Title: Research Scientist and Lecturer, Mechanical Engineering

Thesis Supervisor: Douglas Read  
Title: Associate Professor Maine Maritime Academy



# Contents

<b>1</b>	<b>Background</b>	<b>13</b>
1.1	Motivation . . . . .	13
1.2	Current Tools . . . . .	13
1.3	Resistance . . . . .	14
1.4	Propeller Wake . . . . .	19
<b>2</b>	<b>Analysis</b>	<b>23</b>
2.1	Program Overview . . . . .	23
2.2	Hull . . . . .	24
2.2.1	Hull Coefficients of Form . . . . .	24
2.2.2	Potential Flow . . . . .	24
2.2.3	Boundary Layer . . . . .	27
2.3	Resistance . . . . .	34
2.3.1	Viscous Resistance . . . . .	34
2.3.2	Wave Resistance . . . . .	35
2.3.3	Transom Stern Correction . . . . .	41
2.3.4	Propeller Wake . . . . .	43
<b>3</b>	<b>Results and Discussion</b>	<b>47</b>
3.1	Results . . . . .	47
3.2	Conclusions . . . . .	72



# List of Figures

1-1	Prohaska Method.[8]	16
1-2	Resistance component comparison.	17
1-3	Center Plane source distribution of Michell Integral.[12]	18
1-4	Wake representations, axial velocity.[8]	20
1-5	Wake representations, axial velocity circumferentially averaged.[8]	21
2-1	Double body potential flow.[8]	25
2-2	Physical interpretation for the displacement thickness ( $\delta_1 = \delta^*$ ).[8]	28
2-3	Cole's velocity profile in the turbulent boundary layer.[3]	31
2-4	Results of Corrected Theory training.[12]	39
2-5	Results of Modified Theory training.[12]	41
2-6	Transom stern problem definition.[4]	42
2-7	Boundary layer evaluation points used to determine propeller wake.	45
3-1	Series 60 $C_B = 0.6$ body and profile plans.[14]	48
3-2	Series 60 $C_B = 0.65$ body and profile plans.[14]	49
3-3	Series 60 $C_B = 0.7$ body and profile plans.[14]	50
3-4	Series 60 $C_B = 0.6$ meshed hull.	51
3-5	Series 60 $C_B = 0.65$ meshed hull.	52
3-6	Series 60 $C_B = 0.7$ meshed hull.	53
3-7	Potential flow $C_p$ distribution and body streamlines for use with integral boundary layer calculation for $C_B = 0.6$ . Bow to stern (top), stern to bow (middle), and side view (bottom).	54

3-8	Potential flow $C_p$ distribution along body streamlines for use with integral boundary layer calculation for $C_B = 0.6$ . . . . .	55
3-9	Potential flow $C_p$ distribution and body streamlines for use with integral boundary layer calculation for $C_B = 0.65$ . Bow to stern (top), stern to bow (middle), and side view (bottom). . . . .	56
3-10	Potential flow $C_p$ distribution and body streamlines for use with integral boundary layer calculation for $C_B = 0.70$ . Bow to stern (top), stern to bow (middle), and side view (bottom). . . . .	57
3-11	Skin friction coefficient from the integral boundary layer method compared to ITTC 1957. . . . .	58
3-12	Skin friction $C_f$ distribution from the integral boundary layer solution for $C_B = 0.60$ . . . . .	59
3-13	Boundary layer thickness, $\delta$ , distribution from the integral boundary layer solution for $C_B = 0.60$ . . . . .	60
3-14	Boundary layer displacement thickness, $\delta^*$ , distribution from the integral boundary layer solution for $C_B = 0.60$ . . . . .	61
3-15	Skin friction coefficient comparison of the ATTC and ITTC friction lines.	62
3-16	Form factor calculation comparison. . . . .	64
3-17	Total resistance comparison between extrapolated model test results and prediction for $C_b = 0.6$ with numerical model scale form factor. . . . .	65
3-18	Total resistance comparison between extrapolated model test results and prediction for $C_b = 0.6$ with empirical form factor. . . . .	66
3-19	Total resistance comparison between extrapolated model test results and prediction for $C_b = 0.65$ with numerical model scale form factor. . . . .	67
3-20	Total resistance comparison between extrapolated model test results and prediction for $C_b = 0.65$ with empirical form factor. . . . .	68
3-21	Total resistance comparison between extrapolated model test results and prediction for $C_b = 0.70$ with numerical model scale form factor. . . . .	69
3-22	Total resistance comparison between extrapolated model test results and prediction for $C_b = 0.70$ with empirical form factor. . . . .	70

3-23 Predicted vs measured axial wake velocity contours, $\frac{u}{U}$ .	71
3-24 Predicted vs measured wake from model test.	72



# List of Tables

2.1	Hull Geometric Coefficients of Form . . . . .	24
2.2	Transom stern coefficients for transom-ventilation.[4] . . . . .	43
2.3	Transom stern coefficients for hollow-length.[4] . . . . .	43



# **Chapter 1**

## **Background**

### **1.1 Motivation**

The intent of this thesis is to produce a preliminary design tool that will allow the designer to predict the total resistance and wake characteristics of a given hull form, to be used for global optimization purposes. The efficient computational time will allow the designer to quickly update the design due to changing requirements. Once the optimal hull design is established the designer can move to higher fidelity codes to refine the hull. The tool developed uses a 3D potential flow panel method coupled with an integral boundary layer solver to predict the viscous resistance and propeller wake. The wave drag is calculated using a modified linear theory, thus eliminating the need to run fully three-dimensional potential flow codes. Including an estimate of the propeller wake will allow optimization routines to include the viscous effects of hull shaping, therefore the optimal system or combination of hull and propeller will be obtained for the concept design stage.

### **1.2 Current Tools**

In the framework of early stage hull form optimization, global aspects of the hull performance are of most importance. The local flow characteristics are only of concern when entering the concept design stage. Current tools to determine the flow

characteristics include three dimensional fully viscous CFD codes, based on the solution of the Reynolds Averaged Navier Stokes Equations (RANSE) and potential flow panel-methods. RANSE codes will capture the local flow characteristics but require four orders of magnitude longer computational times than the potential flow panel method and are not required during the preliminary hull form optimization. To obtain an estimate of the wave resistance CFD codes are again used but require an accurate discretized free surface and require longer computational times (on the order of two orders of magnitude, [12]) with respect the method used, even with linearized boundary conditions. Other methods that do not require discretization of the free surface include Michell's Thin-Ship theory and Neumann-Michell theory [6]. The Neumann-Michell theory is computationally efficient but improves the Michell theory exaggeration of the  $F_r vs. C_w$  curve by placing the singularities on the hull surface, instead of the projection of the hull surface on the hull centerplane [6]. To obtain an estimate of the viscous resistance for preliminary design purposes, the use of correlation lines is widely used. Alternatives are to again run a RANSE simulation that can lead to a quite accurate estimation of viscous drag [15]. An alternative to contain computational times is to use an integral boundary layer solver on top of the potential flow body streamlines, as is the approach taken in the code developed here.

### 1.3 Resistance

The resistance of a ship is a combination of a few components, namely the friction, form, and wave drag. In model testing, the measured residual or wave drag coefficient is assumed to be the same as the full scale ship due to testing the model at Froude similitude. Because the models are run at Froude similitude, the Reynolds number of the model and ship do not match, therefore the fictional resistance is determined from a  $C_f$  correlation line for the full scale ship with the form factor determined from the model test. The total resistance of a ship is represented as,

$$R = 0.5 C_T \rho S U^2 \quad (1.1)$$

$C_T$  is the total resistance coefficient of the ship,  $S$  is the surface area and  $U$  is the ship speed. The total resistance coefficient is defined as,

$$C_T = (1 + k) C_f + C_w \quad (1.2)$$

where  $C_f$  and  $C_w$  are the friction and wave resistance coefficients defined as,

$$C_f = \frac{R_f}{0.5\rho SU^2} \quad (1.3)$$

$$C_w = \frac{R_w}{0.5\rho SU^2} \quad (1.4)$$

The frictional resistance of a ship,  $C_f$ , is dependent upon the Reynolds number, a non-dimensional number which relates the inertial and viscous forces.

$$R_e = \frac{UL}{\nu} \quad (1.5)$$

The frictional resistance can either be obtained from a boundary layer code or from model test correlation lines. One popular correlation line is the ITTC 1957 line,

$$C_f = \frac{0.075}{(\log R_e - 2)^2} \quad (1.6)$$

The ITTC 1957 line is developed to represent the frictional resistance of slender ships, and is commonly modified by a form factor,  $1 + k$ , to account for viscous resistance, form drag. Form drag is common with fuller ships that do not experience zero residual resistance at low Froude numbers. The form factor can be determined in several ways. An empirical formula presented by Watanabe [8],

$$k = -0.095 + 25.6 \frac{C_B}{(\frac{L}{B})^2 \sqrt{\frac{B}{T}}} \quad (1.7)$$

The form factor can also be determined using a low speed ( $F_R < 0.15$ ) model test because the wave drag at this low speed becomes negligible. The form factor ( $1 + k$ ) is the ratio of the total resistance to the frictional resistance determined from

a correlation line.

$$\frac{C_T}{C_f} = (1 + k) \quad (1.8)$$

A third method to determine the form factor is Prohaska's Method. The Prohaska Method also relies on a model test, but does not have to be explicitly run at a low Froude number to ensure the wave drag is zero. The Prohaska method is based on the assumption that the wave resistance coefficient is proportional to  $F_r^4$ ,

$$\frac{C_T}{C_f} = (1 + k) + k_1 \frac{F_r^4}{C_f} \quad (1.9)$$

Plotting Prohaska's Method as  $\frac{C_T}{C_f}$  vs.  $\frac{F_r^4}{C_f}$  will result in the measured data falling on a straight line, slope is  $k_1$ , with the intersection of the vertical axis being the value  $1 + k$ . [8]

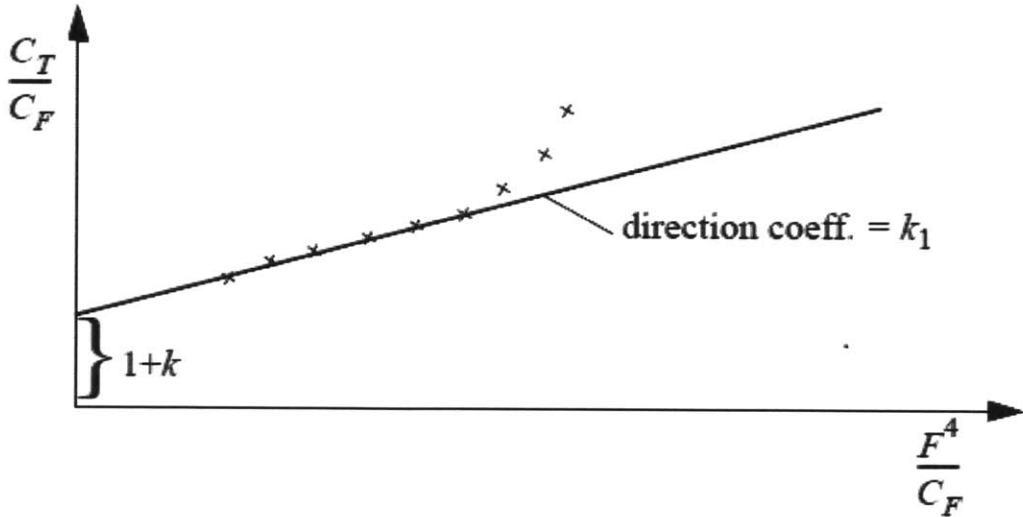


Figure 1-1: Prohaska Method.[8]

The combination of the friction and form drag is known as the viscous drag. In the tool developed the friction resistance is determined from a 2D integral boundary layer solver on the 3D streamlines from the double body solution (no free surface).

The form factor is calculated as a pressure drag when flow separates from the hull.

The non-dimensional wave resistance of a ship,  $C_w$ , is governed by the non-dimensional Froude number which relates the inertial forces to the gravitational forces

$$F_r = \frac{U}{\sqrt{gL}} \quad (1.10)$$

In determining the resistance of a ship, an accurate estimate of the wave drag is essential as it is the dominant resistance component at higher Froude numbers, while viscous effects dominate at low Froude numbers.

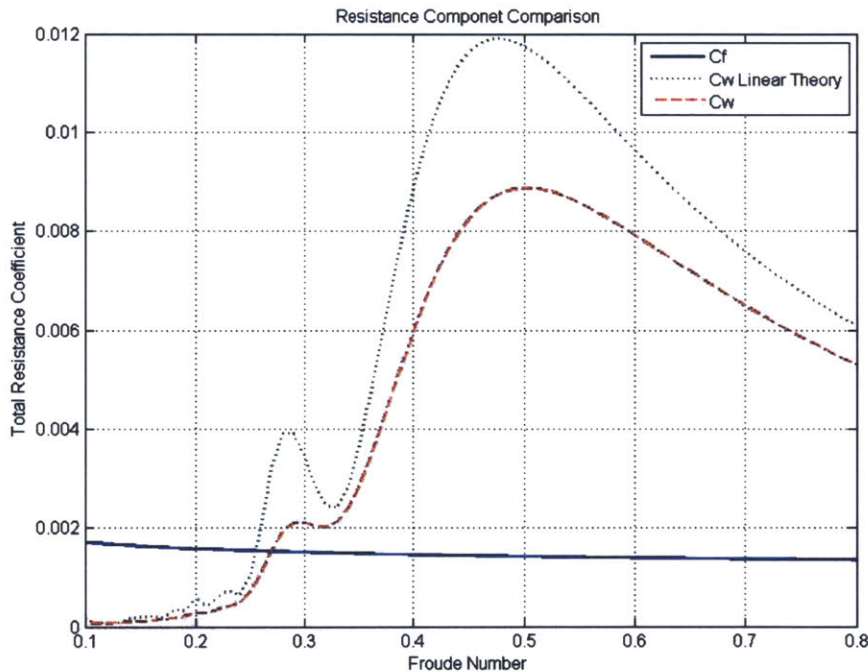


Figure 1-2: Resistance component comparison.

There are a few theoretical/numerical methods to obtain an estimate for the wave resistance of a ship associated with the generation of the free wave pattern, i.e. not accounting for spray or breaking waves. One must either employ a fully 3D free surface boundary element code, rely on model testing, or use the Michell Integral (Linear Theory). None of these methods are optimal for the early stage hull optimization

and design space exploration, as a full 3-D free surface boundary layer code does not execute fast enough to fully explore the design space, model testing requires the construction of many test hulls which can be costly, and Linear Theory tends to exaggerate the peaks in the wave drag vs. Froude number curve. As noted by Read [12], Linear Theory does not do well ranking ships with  $B/T$  greater than 2, which is the ratio for a typical monohull. Read describes the reason is because Linear Theory relies on a centerplane source distribution to represent the hull instead of placing the singularities on the hull surface itself, see Figure 1-3.[12]

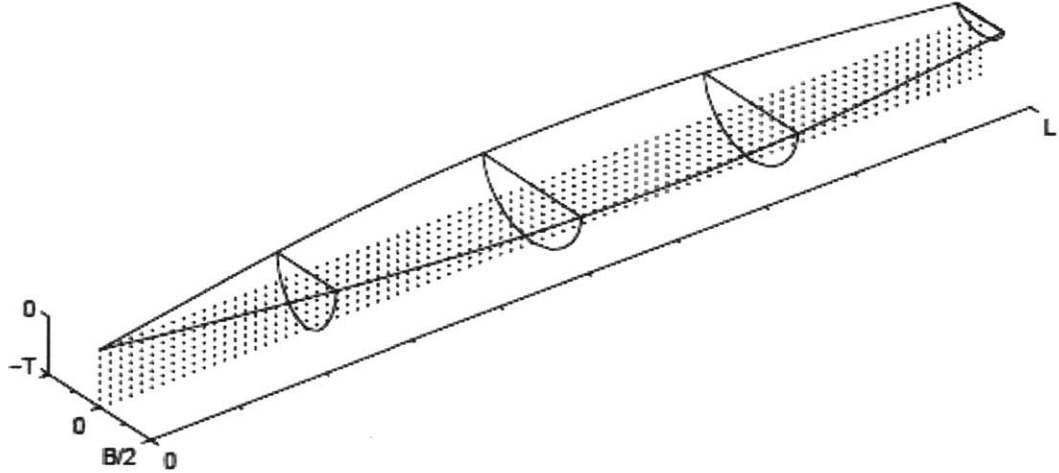


Figure 1-3: Center Plane source distribution of Michell Integral.[12]

The Michell Integral is defined as [5],

$$R = \frac{\pi}{2} \rho U^2 \int_{-\frac{\pi}{2}}^{\frac{\pi}{2}} |A(\theta)|^2 \cos^3 \theta d\theta \quad (1.11)$$

$|A(\theta)|$  is the complex amplitude function or the free wave spectrum. The solution to the Michell integral with the free wave spectrum is detailed in Chapter 2. The code developed uses the Michell Integral (Linear Theory) to determine the wave resistance with the modification made by Read [12] to eliminate the exaggerated peaks in the

Linear Theory wave resistance solution.

## 1.4 Propeller Wake

Another important aspect in hull design is optimizing the propeller wake in order to maximize the propeller efficiency and propulsive efficiency of the hull/propeller system. To maximize the efficiency of the hull/propeller system, the wake fraction is important as it is part of the hull efficiency definition. The hull efficiency is defined as the resistance of the ship times the forward speed divided by the actual thrust the propeller must deliver to propel the ship at velocity  $V$  with an inflow velocity to the propeller of  $V_a$ , the advance velocity.

$$\eta_H = \frac{R_T V}{T V_a} = \frac{1 - t}{1 - w} \quad (1.12)$$

where  $t$  is the thrust deduction factor and  $w$  is the wake fraction. If the designer does not consider the hull efficiency they may optimize the resistance of just the ship at the expense of an efficient propeller, reducing the overall system efficiency.

Due to the boundary layer around the hull, the inflow velocity to the propeller is less than the ship's speed, where the wake fraction is defined as,

$$w = 1 - \frac{V_a}{V_s} \quad (1.13)$$

Contours of the axial inflow velocity to the propeller with respect to the ship speed are shown in Figure 1-4. Figure 1-4 also shows the angular variation of the axial inflow velocity for specific radii within the propeller disk.

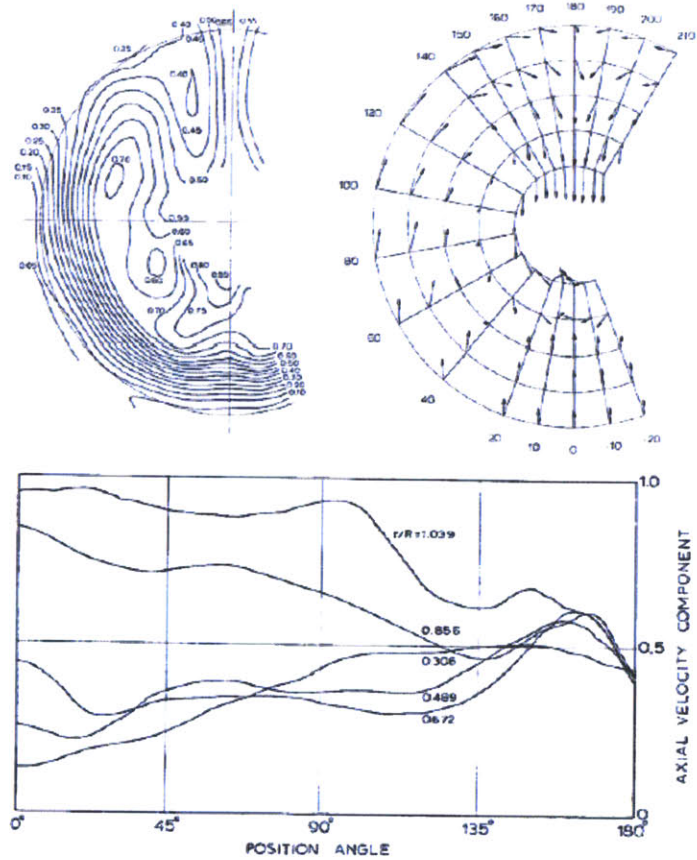


Figure 1-4: Wake representations, axial velocity.[8]

The propeller wake can be averaged circumferentially at each radius to aid in designing a wake adapted propeller, as shown in Figure 1-5 where the nominal inflow is the flow without a propeller and the effective inflow includes the effects of the propeller present in the wake.

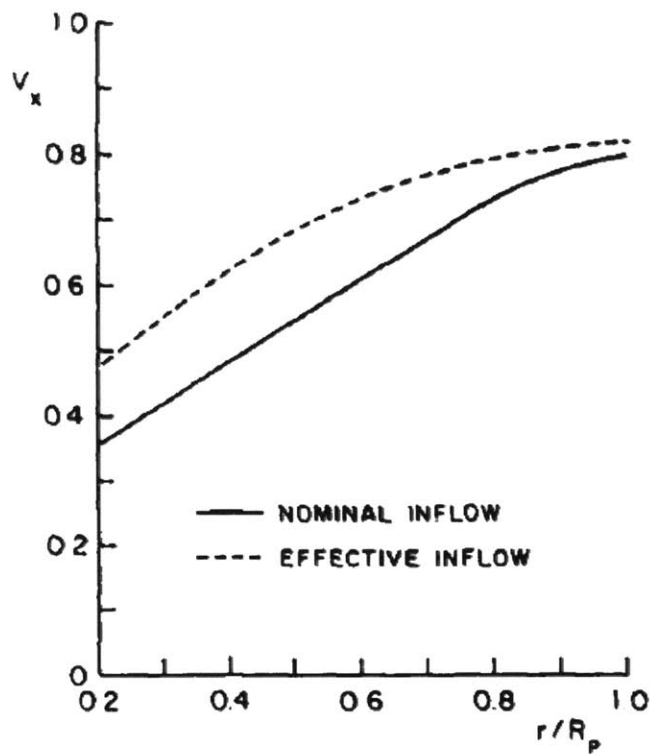


Figure 1-5: Wake representations, axial velocity circumferentially averaged.[8]

To calculate the wake in the code developed, the integral boundary layer solution is solved to determine the boundary layer characteristics, then the Preitsch [11] profile is assumed for the velocity distribution within the boundary layer . The velocity within the boundary layer is circumferentially averaged at each radius to calculate the wake fraction,  $w$ . Details of the wake fraction calculation are expanded upon in Section 2.3.4.



# **Chapter 2**

## **Analysis**

### **2.1 Program Overview**

The tool developed to predict the resistance and propeller wake of a ship is designed to execute quickly, therefore fully viscous effects are not captured in the analysis as the flow is obtained from a 3-D potential flow solver coupled with a 2-D integral boundary layer solver. The program is broken into two modules:

1. Hull Module.
2. Resistance Module.

The Hull Module takes a meshed hull and produces the required hull geometric coefficients of form, the hull wetted surface area, and potential flow solution. The results from the Hull Module are passed to the Resistance Module for input to an integral boundary layer solver and wave drag estimation and corrections. The integral boundary layer solver is used to predict the frictional resistance and propeller wake.

## 2.2 Hull

### 2.2.1 Hull Coefficients of Form

The hull module of the program is used to determine the hull geometric coefficients of form and surface area from the meshed hull. The hull form coefficients and surface area are passed to the Resistance Module to determine the total resistance. The Prismatic, Volumetric, Max Section, and  $\frac{B}{T}$  are the coefficients the Hull Module calculates and are defined in Table 2.1.

Table 2.1: Hull Geometric Coefficients of Form

Coefficient	Equation
Prismatic	$C_p = \frac{\nabla}{A_x L}$
Volumetric	$C_v = \frac{\nabla}{L^3}$
Max Section	$C_x = \frac{\nabla}{BT}$

### 2.2.2 Potential Flow

Due to the computational time requirements of running a full free surface RANSE calculation, this code has chosen to use a double body solution, i.e. no free surface, with an integral boundary layer solver since the wave drag will come from Corrected or Modified Linear Theory [12]. Using the double body solution will significantly increase the speed of the program and allow for greater design space exploration. Figure 2-1 shows the general double body potential flow problem where the traditional free surface is a fixed symmetry plane.

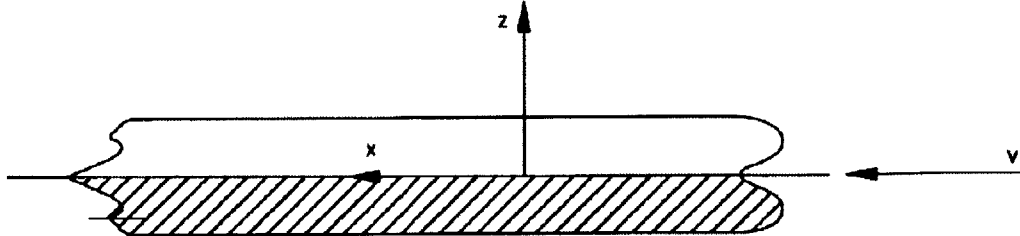


Figure 2-1: Double body potential flow.[8]

The general equation for incompressible potential flow is,

$$\frac{d^2\phi}{dx^2} + \frac{d^2\phi}{dy^2} + \frac{d^2\phi}{dz^2} = 0 \quad (2.1)$$

To solve the Laplace equation the flow field must be represented by singularities. For a non-lifting body such as a hull, the singularities used to represent the body are sources. A source's potential and flow field are defined as,[8]

$$\phi(\vec{x}) = -\frac{Q}{4\pi R} \quad (2.2)$$

$$v(\vec{x}) = \frac{Q}{4\pi R^2} \quad (2.3)$$

When the hull is placed in the presence of an oncoming uniform flow, the potential and velocity field of the hull and uniform flow are superimposed to produce the complete flow field [8].

$$\phi(\vec{x}) = \vec{U}_\infty \cdot \vec{x} - \frac{Q}{4\pi R} \quad (2.4)$$

$$v(\vec{x}) = \vec{U}_\infty + \frac{Q}{4\pi R^2} \quad (2.5)$$

To solve the potential flow problem, the hull is discretized into panels, this is known as the panel method. With this method singularities (in this case sources) are

placed on the intended hull surface at the discretized panel centers. Every panel is given a source strength, which can either be constant or vary linearly over the panel. With the sources placed on the intended hull surface, the potential and velocity field of the induced flow in a uniform flow is now,

$$\phi(\vec{x}) = \vec{U}_\infty \cdot \vec{x} - \frac{1}{4\pi} \int \int_S \frac{\sigma(\vec{\xi})}{R} dS \quad (2.6)$$

$$v(\vec{x}) = \vec{U}_\infty + \int \int_S \frac{\sigma(\vec{\xi})}{4\pi R^3} \cdot (\vec{x} - \vec{\xi}) dS \quad (2.7)$$

where  $R = |\vec{x} - \vec{\xi}|$  and  $\xi$  is the singularity location.

Discretizing the hull surface into  $N$  panels, the velocity field equation becomes,

$$v(\vec{x}) = \vec{U}_\infty + \sum_{j=1}^N \sigma_j \int \int_{S_j} \frac{(\vec{\xi})}{4\pi R^3} \cdot (\vec{x} - \vec{\xi}) dS \quad (2.8)$$

$$v(\vec{x}) = \vec{U}_\infty + \sum_{j=1}^N \sigma_j \cdot V_j(\vec{x}) \quad (2.9)$$

where  $V_j$  is the influence coefficient vector. The influence coefficient vector corresponds to the velocity induced at point  $x$  due to the source located on panel  $j$ .

The source strengths are solved given the boundary condition that the flow through the hull surface must be zero,[8]

$$\vec{v} \cdot \vec{n} = \frac{d\phi}{dn} = 0 \quad (2.10)$$

The boundary condition is enforced at a discrete set of collocation points, usually the panel centers. Substituting the velocity flow field into the boundary condition,

$$\sum_{j=1}^N \sigma_j \cdot V_j(\vec{x}_i) = -\vec{U}_\infty \cdot \vec{n}_i \quad (2.11)$$

Equation 2.11 forms a set of  $N$  equations with  $N$  unknowns from which the source strengths,  $\sigma_j$ , are solved. Knowing the source strengths, the complete potential and velocity fields are known from which the pressure field can be calculated by the

Bernoulli equation,

$$\frac{1}{2} \nabla \phi \cdot \nabla \phi + \frac{p}{\rho} + gz = \text{constant} \quad (2.12)$$

From the potential flow solution the streamlines are traced for performing a 2D integral boundary layer solution on top of the 3D streamlines. The streamlines are traced by solving an ordinary differential equation because the velocity vector,  $\vec{v}$ , is known at an arbitrary point  $\vec{P}$  [13]. The coordinates of a velocity streamline are parameterized by  $t$ , to obtain  $\vec{P}(t)$ . The tangent vector to the streamline is then [13],

$$\frac{d\vec{P}}{dt} = g(t)\vec{V}(\vec{P}(t)) \quad (2.13)$$

The function  $g(t) \equiv 1$  by convention. Given an initial point  $\vec{P}_0$  on a velocity streamline, the streamline is traced by solving the initial value problem [13],

$$\frac{d\vec{P}}{dt} = \vec{V}_\infty + \vec{v}(\vec{P}(t)) \quad (2.14)$$

where,

$$\vec{P}(0) = \vec{P}_0 \quad (2.15)$$

### 2.2.3 Boundary Layer

From the potential flow solution of the double body model and body streamlines, the boundary layer is solved to determine both the frictional resistance and boundary layer characteristics for use in calculating the propeller wake and form drag. The boundary layer is solved using an integral boundary layer method on the body streamlines. The flow around the ship is assumed turbulent, therefore only the turbulent boundary layer is considered. The characteristics of a boundary layer include the thickness, displacement thickness, and momentum thickness. The thickness of the boundary layer is typically defined as the thickness where the velocity within the boundary layer reaches a percentage of the potential flow velocity, typically  $\delta_{99\%}$  or

$\delta_{99.5\%}$ .

The displacement thickness is defined as,

$$\delta^* = \int_0^\delta \left(1 - \frac{u}{U}\right) dy \quad (2.16)$$

The physical interpretation of the displacement thickness is that it is the virtual thickening of the body represented in a potential flow solution. Within the displacement thickness the velocity is zero, and outside the displacement thickness is equal to the velocity outside the boundary layer. Figure 2-2 illustrates the physical interpretation of the displacement thickness.

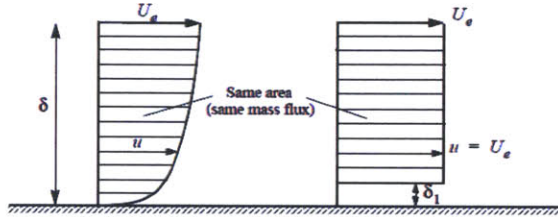


Figure 2-2: Physical interpretation for the displacement thickness ( $\delta_1 = \delta^*$ ).[8]

The momentum thickness is defined as,

$$\theta = \int_0^\delta \frac{u}{U} \left(1 - \frac{u}{U}\right) dy \quad (2.17)$$

The momentum thickness is often used in measuring the resistance of an object.

Another important quantity from the boundary layer solution is the local friction coefficient, defined as,

$$c_f = \frac{\tau_w}{\frac{1}{2} \rho u^2} \quad (2.18)$$

where  $\tau_w$  is the local wall shear stress,

$$\tau_w = \mu \frac{du}{dy} \Big|_{y=0} \quad (2.19)$$

The general 2D turbulent boundary layer equations, assuming the flow is incompressible, has constant dynamic viscosity, and has been time averaged (2D Reynolds averaged Navier-Stokes equations) are,

$$u \frac{\partial u}{\partial x} + v \frac{\partial u}{\partial y} = -\frac{1}{\rho} \frac{\partial p}{\partial x} + \frac{\mu}{\rho} \left( \frac{\partial^2 u}{\partial x^2} + \frac{\partial^2 u}{\partial y^2} \right) - \left( \frac{\partial \bar{u}' u'}{\partial x} \frac{\partial \bar{u}' u'}{\partial y} \right) \quad (2.20)$$

$$u \frac{\partial v}{\partial x} + v \frac{\partial v}{\partial y} = -\frac{1}{\rho} \frac{\partial p}{\partial y} + \frac{\mu}{\rho} \left( \frac{\partial^2 v}{\partial x^2} + \frac{\partial^2 v}{\partial y^2} \right) - \left( \frac{\partial \bar{u}' v'}{\partial x} \frac{\partial \bar{v}' v'}{\partial y} \right) \quad (2.21)$$

The effects of curvature are neglected because the curvature effects on moderately curved surfaces are negligible. This is a source of error especially in the stern of some ships where the curvature is significant. To simplify the boundary layer equations dimensional analysis is employed. The thickness of the boundary layer,  $\delta$ , is much smaller in magnitude when compared to the length along which the boundary layer forms,  $\delta \ll l$ , simplifying the turbulent boundary layer equations to,

$$u \frac{\partial u}{\partial x} + v \frac{\partial u}{\partial y} = -\frac{1}{\rho} \frac{\partial p}{\partial x} + \frac{\mu}{\rho} \left( \frac{\partial^2 u}{\partial y^2} \right) - \left( \frac{\partial \bar{u}' u'}{\partial y} \right) \quad (2.22)$$

$$\frac{\partial p}{\partial y} = 0 \quad (2.23)$$

To obtain the integral boundary layer equations, the differential boundary layer equations are integrated from the surface to  $\delta$ , the boundary layer thickness.

The two turbulent boundary layer equations are subject to the no slip condition and that the internal boundary layer velocity must equal the potential flow velocity at  $y = \delta$ , explicitly,

$$y = 0 \quad u = v = 0 \quad (2.24)$$

$$y = \delta \quad u = U(x) \quad (2.25)$$

To solve the boundary layer, an integral boundary layer solution is employed,

specifically the method of Nash and Hicks, along each streamline[10]. Multiplying the continuity equation by  $y^\alpha$  and integrating from 0 to the boundary layer thickness,  $\delta$ , yields a family of integral equations,

$$\int_0^\delta y^\alpha u \frac{\partial u}{\partial x} \delta y - \int_0^\delta \left[ y^\alpha u \frac{\partial u}{\partial y} \left( \int_0^y \frac{\partial u}{\partial x} \right) \right] \delta y = \frac{\delta^{\alpha+1}}{\alpha+1} U \frac{\partial U}{\partial x} + \frac{1}{\rho} \int_0^\delta y^\alpha \frac{\partial \tau}{\partial y} \delta y \quad (2.26)$$

$$\tau = \mu \frac{\partial u}{\partial y} - \rho \bar{u}' v' \quad (2.27)$$

To solve the integral equation Nash and Hicks used the Cole's velocity profile, shown in Figure 2-3 [10],

$$u(y) = \frac{u_\tau}{\kappa} \left[ \ln(y \frac{u_\tau}{\nu}) + 5\kappa \right] + \frac{u_\beta}{2} \left[ 1 - \cos \left( \frac{\pi y}{\delta} \right) \right] \quad (2.28)$$

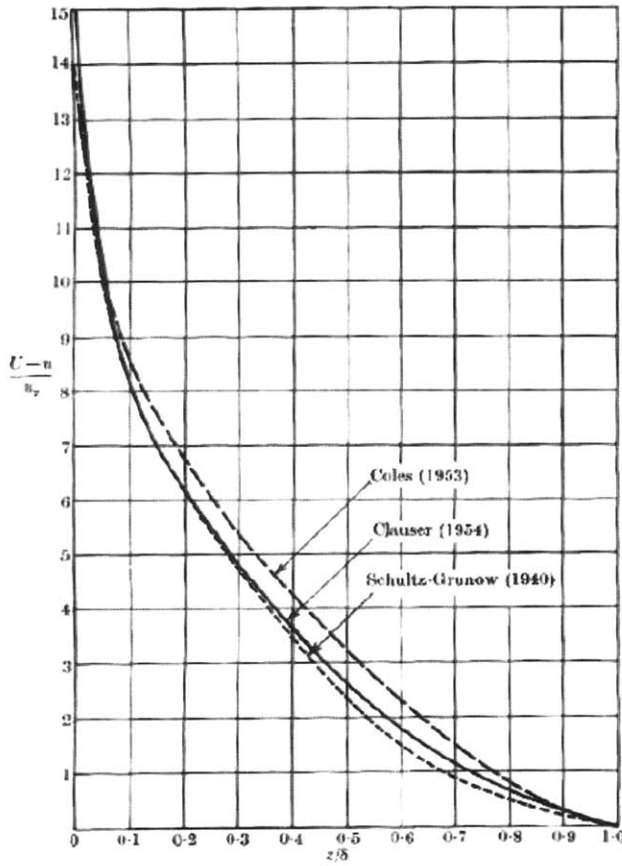


Figure 2-3: Cole's velocity profile in the turbulent boundary layer.[3]

The integral quantities are derived for the method of Nash and Hicks by integrating the Cole's velocity profile,

$$\frac{\delta^*}{\delta} = \frac{1}{\kappa} \frac{u_\tau}{U} + \frac{1}{2} \frac{u_\beta}{U} \quad (2.29)$$

$$\frac{\theta}{\delta} = \frac{\delta^*}{\delta} - \left[ \frac{2}{\kappa^2} \left( \frac{u_\tau}{U} \right)^2 + \frac{3}{8} \left( \frac{u_\beta}{U} \right)^2 + \frac{1.58949}{\kappa} \frac{u_\tau u_\beta}{U^2} \right] \quad (2.30)$$

The integral quantities from the Cole's velocity profile are substituted into the momentum equations to yield,

$$F_1 \frac{1}{\delta} \frac{d\delta}{dx} + F_2 \frac{du_\beta}{dx} + F_3 \frac{du_\tau}{dx} = F_4 \frac{dU}{dx} + \phi \quad (2.31)$$

The coefficients  $F_1$  through  $F_4$  are dependent upon the value of  $\alpha$ , which form a

system of equations which are numerically integrated.

When  $\alpha = 0$ , the momentum integral equation is obtained with the following coefficients,

$$\begin{aligned}
 F_1 &= \left[ \frac{3}{8}u_\beta^2 - \frac{1}{2}Uu_\beta + 2\frac{u_\tau^2}{\kappa^2} + 1.58949u_\beta\frac{u_\tau}{\kappa} - \frac{Uu_\tau}{\kappa} \right] \\
 F_2 &= \left[ \frac{3}{4}u_\beta - \frac{1}{2}U + 1.58949u_\beta\frac{u_\tau}{\kappa} \right] \\
 F_3 &= \frac{1}{\kappa} \left[ 4\frac{u_\tau}{\kappa} + 1.58949u_\beta - U \right] \\
 F_4 &= \left[ u_\beta + 2\frac{u_\tau}{\kappa} \right] \\
 \phi &= -\frac{u_\tau^2}{\delta}
 \end{aligned} \tag{2.32}$$

When  $\alpha = 1$ , the moment of the momentum integral equation is obtained with the following coefficients,

$$\begin{aligned}
 F_1 &= u_\beta^2 \left( \frac{5}{16} - \frac{1}{\pi^2} \right) - Uu_\beta \left( \frac{1}{2} - \frac{2}{\pi^2} \right) + \frac{3}{4}\frac{u_\tau^2}{\kappa^2} + \frac{u_\beta u_\tau}{\kappa} \left( \frac{3}{4} + \frac{2}{\pi^2} - 0.16701 \right) - \frac{1}{2}U\frac{u_\tau}{\kappa} \\
 F_2 &= u_\beta^2 \left( \frac{1}{2} - \frac{2}{\pi^2} \right) - U \left( \frac{1}{4} - \frac{1}{\pi^2} \right) + \frac{u_\tau}{\kappa} \left( \frac{3}{8} + \frac{2}{\pi^2} - \frac{0.16701}{2} \right) \\
 F_3 &= \frac{u_\tau}{\kappa^2} + \frac{u_\beta}{\kappa} \left( \frac{5}{8} + \frac{2}{\pi^2} \right) - \left( \frac{3}{2}0.16701 \right) - \frac{U}{4\kappa} \\
 F_4 &= u_\beta \left( \frac{3}{4} - \frac{3}{\pi^2} \right) + \frac{3}{4}\frac{u_\tau}{\kappa} \\
 \phi &= -\frac{1}{2}C_\tau\frac{U^2}{\delta}
 \end{aligned} \tag{2.33}$$

When  $\alpha = \infty$ , the differentiated skin friction law is obtained with the following coefficients,

$$\begin{aligned}
 F_1 &= \frac{u_\tau}{\kappa} \\
 F_2 &= 1.0
 \end{aligned}$$

$$\begin{aligned}
F_3 &= \frac{1}{\kappa} \left[ \ln \left( \frac{u_\tau \delta}{\nu} \right) + 1.0 + C \right] \\
F_4 &= 1.0 \\
\phi &= 0.0
\end{aligned} \tag{2.34}$$

To close the set of three equations, another equation is needed to solve for the four unknowns,  $u_\tau, u_\beta, \delta, C_\tau$ .

$$\frac{dC_\tau}{dx} = \frac{\lambda}{\delta} (\hat{C}_\tau - C_\tau) \tag{2.35}$$

where

$$C_\tau = \frac{1}{\frac{1}{2}\rho U^2 \delta} \int_0^\delta \tau dy \tag{2.36}$$

The values of  $\lambda$  and  $\hat{C}_\tau$  are determined empirically,

$$\lambda = 0.15 \tag{2.37}$$

$$\hat{C}_\tau = 0.025 \left( 1.0 - \frac{1.0}{H} \right)^2 \tag{2.38}$$

Where  $H$  is the shape factor,

$$H = \frac{1.4754}{\log_{10}(Re_\theta)} + 0.9698 \tag{2.39}$$

and  $\kappa$  is the Von Karman constant equal to 0.41.

The momentum equations are solved with an iterative solution along each stream-line to determine the boundary layer characteristics and local skin friction coefficient. If a laminar boundary layer solution preceded, the values for the boundary layer characteristics and local skin friction at the transition point would be the initial guesses for the turbulent boundary layer, otherwise initial guesses must be supplied.[10][1]

## 2.3 Resistance

### 2.3.1 Viscous Resistance

The viscous resistance is comprised of both the frictional resistance and form drag.

#### Frictional Resistance

The frictional resistance is calculated from the local skin friction coefficients obtained from the integral boundary layer solution on each streamline. The local skin friction coefficients are mapped to the centers of each panel on the hull. The friction coefficient calculated in the boundary layer analysis is the friction in the direction of the streamline, therefore only the local x-component of the friction is used in the total skin friction calculation. The total skin friction resistance is,

$$R_f = 0.5\rho U^2 \sum_{i=0}^N c_f A_i \cdot n_{x,i} \quad (2.40)$$

where N is the number of panels defining the hull.

#### Form Drag

The form drag is calculated when the flow separates from the hull by considering the hull curvature in the direction of the streamline and the pressure as it changes along the streamline. Separation typically occurs in viscous flows in the presence of a strong positive pressure gradient along the surface, slowing the inner layers [2]. When the flow separates, the coefficient of pressure,  $C_p$  is assumed constant from that point aft. The form drag is calculated as a pressure force,

$$R_{form} = PA \quad (2.41)$$

where the pressure (P) is the dynamic pressure based on the velocity difference from the potential flow solution,

$$P = \frac{1}{2}\rho\delta u_l^2 \quad (2.42)$$

The velocity difference is determined from the coefficient of pressure,  $C_p$ , before and after separation

$$\delta u_t^2 = U^2 \left( C_{p_{sep}} - C_{p_{pflow}} \right) \quad (2.43)$$

The form drag is calculated over the panels in which the flow is separated by summing the force each panel contributes in the x-direction.

$$R_{form} = 0.5\rho U^2 \sum_{i=0}^{N_{sep}} \left( C_{p_{sep}} - C_{p_{pflow}} \right) A_i \cdot n_{x,i} \quad (2.44)$$

The form factor,  $k$ , is calculated as the ratio of the form drag to the frictional drag,

$$k = \frac{R_{form}}{R_f} \quad (2.45)$$

### 2.3.2 Wave Resistance

The wave resistance is calculated by the Michell Integral (Linear Theory) and corrected/modified based on the hull geometric coefficients of form and Froude number [12]. The Michell Integral for wave resistance is based on Thin-Ship Theory which linearizes the hull boundary condition and imposes the boundary conditions on the hull centerplane rather than at the hull surface.

#### Thin-Ship Theory

The potential for a ship moving at velocity  $U$  in the x-direction is,

$$\Phi(x, y, z) = Ux + \phi(x, y, z) \quad (2.46)$$

The gradient of the potential describes the flow field,

$$\nabla\Phi(x, y, z) = \left( U + \frac{\partial\phi}{\partial x} \right) \hat{i} + \frac{\partial\phi}{\partial y} \hat{j} + \frac{\partial\phi}{\partial z} \hat{k} \quad (2.47)$$

The flow must satisfy both the Laplace equation and the Neumann boundary condition of no flow through the hull,

$$\nabla^2 \Phi(x, y, z) = \frac{\partial^2 \phi}{\partial x^2} + \frac{\partial^2 \phi}{\partial y^2} + \frac{\partial^2 \phi}{\partial z^2} \quad (2.48)$$

$$\vec{n} \cdot \nabla \Phi = 0 \quad (2.49)$$

The Neumann boundary condition defines the vector on the hull as,

$$\vec{n} = \left[ \frac{\partial Y}{\partial x}, -1, \frac{\partial Y}{\partial z} \right] \quad (2.50)$$

where  $Y(x, z)$  defines the hull surface. This yields,

$$\frac{\partial \phi}{\partial y} = \left[ U + \frac{\partial \phi}{\partial x} \right] \frac{\partial Y(x, z)}{\partial x} + \frac{\partial \phi}{\partial z} \frac{\partial Y(x, z)}{\partial z} \quad (2.51)$$

which is valid on the hull surface. Thin-ship uses a linearized condition on the hull center-plane to yield the Michell boundary condition,

$$\frac{\partial \phi}{\partial y} = U \frac{\partial Y(x, z)}{\partial x} \quad \text{on } y = 0 \quad (2.52)$$

The second boundary states the velocity potential approaches zero as  $z$  goes to  $-\infty$

The third boundary condition applies the Neumann condition of no flow through the free surface and the Bernoulli equation on the free surface. The Neumann condition gives,

$$\vec{n} = \left[ \frac{\partial Z}{\partial x}, \frac{\partial Z}{\partial y}, -1 \right] \quad (2.53)$$

$$\frac{\partial \phi}{\partial z} = \left[ U + \frac{\partial \phi}{\partial x} \right] \frac{\partial Z(x, z)}{\partial x} + \frac{\partial \phi}{\partial y} \frac{\partial Z(x, z)}{\partial y} \quad (2.54)$$

The Bernoulli equation is,

$$gZ(x, y) + \frac{1}{2} \left[ \left( U + \frac{\partial \phi}{\partial x} \right)^2 + \left( \frac{\partial \phi}{\partial y} \right)^2 + \left( \frac{\partial \phi}{\partial z} \right)^2 \right] = \frac{1}{2} U^2 \quad (2.55)$$

For Linear Theory the velocity squared terms are ignored, resulting in a simplified Bernoulli equation,

$$Z(x, y) = -\frac{U}{g} \frac{\partial \phi}{\partial x} \quad (2.56)$$

Differentiating the simplified Bernoulli equation with respect to  $x$  and  $y$ ,

$$\frac{\partial Z(x, y)}{\partial x} = -\frac{U}{g} \frac{\partial^2 \phi}{\partial x^2} \quad (2.57)$$

$$\frac{\partial Z(x, y)}{\partial y} = -\frac{U}{g} \frac{\partial}{\partial y} \left( \frac{\partial \phi}{\partial x} \right) \quad (2.58)$$

Substituting 2.57 and 2.58 into 2.54,

$$\frac{\partial \phi}{\partial z} = \left[ U + \frac{\partial \phi}{\partial x} \right] \left( -\frac{U}{g} \frac{\partial^2 \phi}{\partial x^2} \right) + \frac{\partial \phi}{\partial y} \left( -\frac{U}{g} \frac{\partial^2 \phi}{\partial y \partial x} \right) \quad (2.59)$$

In Linear Theory only the linear terms remain and the boundary condition is moved to the undisturbed free surface ( $z = 0$ ), yielding the Stokes Boundary condition,

$$\frac{\partial \phi}{\partial z} + \frac{U^2}{g} \frac{\partial^2 \phi}{\partial x^2} = 0 \quad (2.60)$$

### Free Wave Spectrum

The Free-Wave Spectrum,  $|A(\theta)|$ , in infinite depth is defined as [5],

$$A(\theta) = -\frac{2i}{\pi} k_0^2 \sec^4 \theta [P(\theta) + iQ(\theta)] \quad (2.61)$$

$|P(\theta)|$  and  $|Q(\theta)|$  are defined as,

$$P(\theta) = \int F(x, \theta) \cos(k_0 x \sec \theta) dx \quad (2.62)$$

$$Q(\theta) = \int F(x, \theta) \sin(k_0 x \sec \theta) dx \quad (2.63)$$

The function's  $|P(\theta)|$  and  $|Q(\theta)|$  are integrated from bow to stern.

$|F(x, \theta)|$  is defined as,

$$F(\theta) = \int Y(x, z) \exp(k_0 z \sec^2 \theta) dz \quad (2.64)$$

where the offsets  $Y(x, z)$  are the half breadths of the hull and the function is integrated in the vertical *z-direction* from the keel to the free surface,  $z = 0$ , with  $k_0 = \frac{g}{U^2}$ .

The wave resistance is calculated using 1.11 by the numerical method of Tuck, Lazaukas, and Scullen. [5]

### Linear Theory Improvement

As Figure 1-2 shows, Linear Theory exaggerates the peaks of the wave resistance vs. Froude number curve. Read [12] corrects the linear theory results to a set of panel code results by two methods. The two Methods are referred to as *Corrected Theory* and *Modified Theory*. Both methods use the B/T, Volumetric, Maximum Section, and Prismatic hull coefficients to correct/modify the linear theory results. The two methods differ in that the Corrected Theory corrects the linear theory result at every Froude number and therefore requires Froude number as an input. The Modified Theory applies to the entire Froude number range and therefore does not require Froude number as an input. Both Methods are based on training a Neural network using boundary element code results of a fixed hull, i.e. the hull is *not* free to sink and trim. The two methods may be used with a model free to sink and trim by providing the new submerged geometry of the hull to either method. Both methods are trained

using the Taylor Series hull form and provide a significant reduction in computational time versus boundary element methods. Read's corrections retain the speed of linear theory, providing a computational time reduction of three-orders of magnitude when compared to the fully non-linear CFD case. If the linear CFD solution is acceptable, i.e. the free surface is not iterated upon, there is a two-order of magnitude reduction in computational time. [12]

### Corrected Theory

The Corrected Theory is straight forward in that a scale factor is applied to the Linear Theory result as determined through the Neural Network training. Figure 2-4 shows the typical results of the Corrected Theory correction,  $C_w$  Ratio, for a specified  $C_v$ ,  $C_x$ , and  $C_p$  combination.

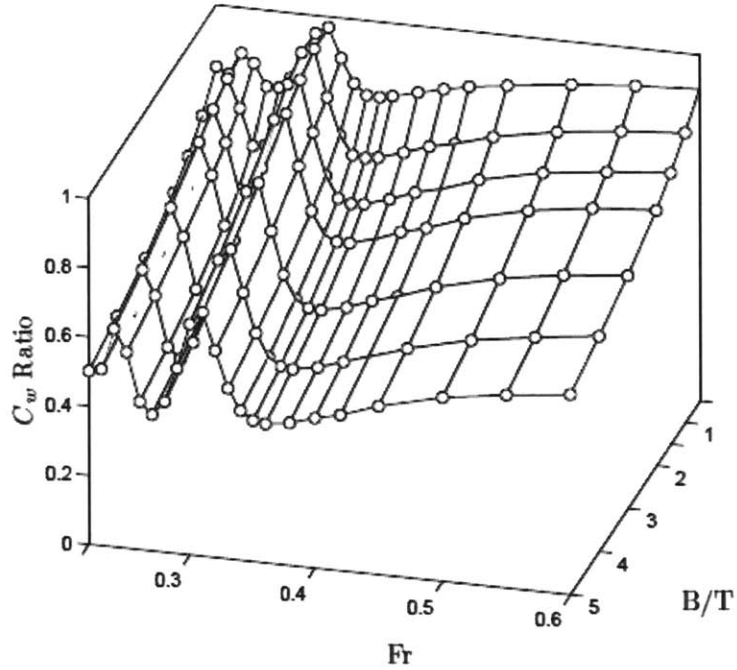


Figure 2-4: Results of Corrected Theory training.[12]

## Modified Theory

Modified Theory reduces the neural network complexity by eliminating Froude number as an input. The Froude number is eliminated from the network by going back to the boundary conditions from which Linear Theory is derived and adding a correction term that will work at all Froude numbers. The linearized boundary condition from which the Michell Integral is based is,

$$k_0\phi_z + \phi_{xx} = 0 \text{ on } z = 0; \quad (2.65)$$

Read revisited the full free surface boundary condition derived from the Bernoulli and Neumann condition to find a term with unknown constants to be trained in a Neural Network with boundary element code results [12]. Read experimented with various terms in the full boundary condition to find one that altered the wave drag in the desired manner, resulting in the new boundary condition,

$$k_0\phi_z + \phi_{xx} + \frac{1}{U^2}\phi_y^2\phi_{yy} = 0 \text{ on } z = 0; \quad (2.66)$$

Read linearizes the  $\phi_y^2$  term assuming it is a function of the hull coefficients. The function is determined with the training data. Read trains the Modified Theory with two correction coefficients,  $C_1$  and  $C_2$  as shown in Figure 2-5 [12].

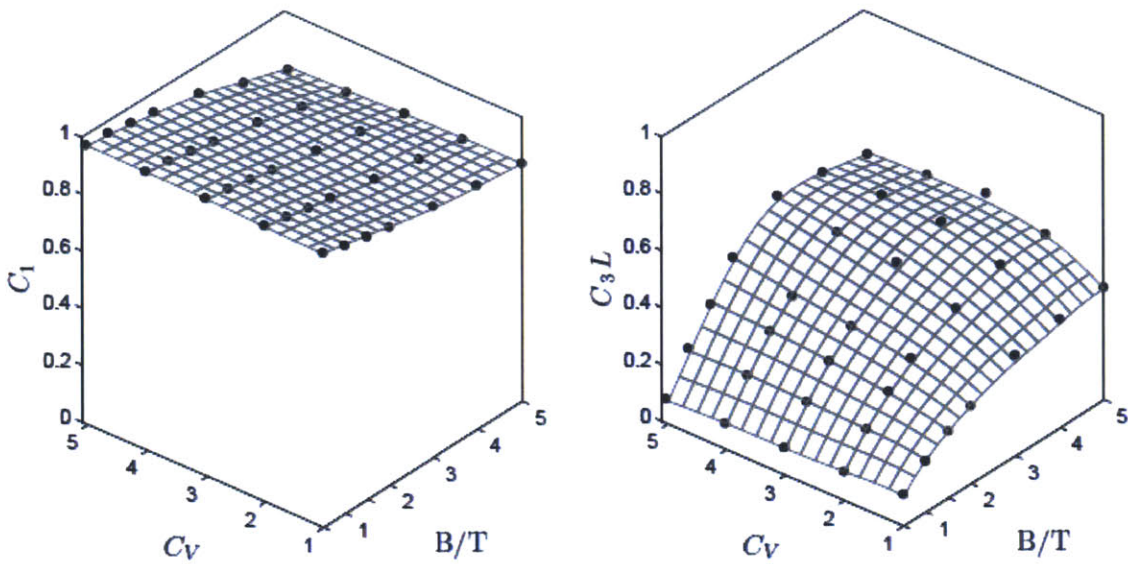


Figure 2-5: Results of Modified Theory training.[12]

The behavior of both correction methods is shown in the results section of Chapter 3.

### 2.3.3 Transom Stern Correction

The use of the Michell Integral requires that the hull closes, i.e. there is no transom stern. To calculate the wave drag of a hull with a transom stern, the hollow left behind the transom stern hull is modeled as an extension of the hull that closes. Doctors [4] performed model tests of transom stern ships to form equations based on a regression analysis to model the hollow left behind the ship.

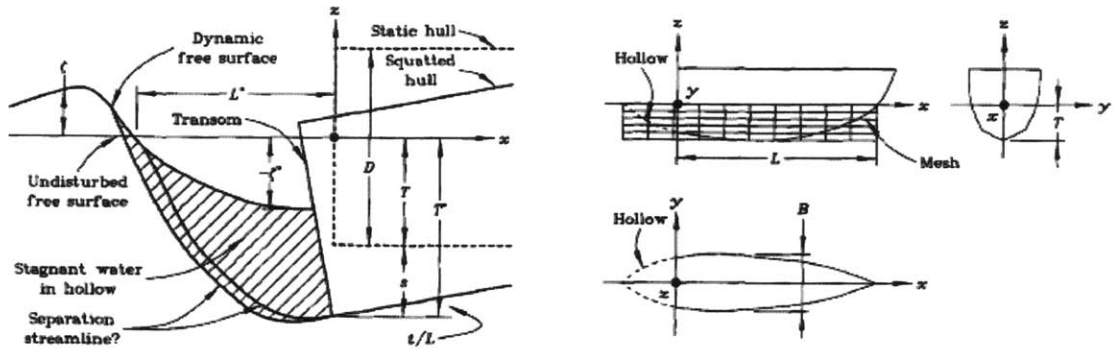


Figure 2-6: Transom stern problem definition.[4]

With the geometry of the hollow defined, the ships transom can be modified to close at the stern with the geometry of the hollow. Doctors study yielded two formulas, one that represents the ventilated portion of the transom ( $\zeta^*$ ) and another that represents the hollow length ( $L^*$ ).

$$-\frac{\zeta^*}{T} = C_1 F_{nT}^{C_2} \left(\frac{B}{T}\right)^{C_3} R_{nT}^{C_4} \quad (2.67)$$

$$\frac{L^*}{T} = C_1 F_{nT}^{C_2} \left(\frac{B}{T}\right)^{C_3} R_{nT}^{C_4} \quad (2.68)$$

In the above equations,  $T$  is the draft of the transom,  $F_{nT}$  and  $R_{nT}$  are the Froude and Reynolds numbers based on the transom draft, respectfully. The coefficients for the regressions depend on the number of coefficients used in the fit and whether the analysis is for a static or dynamic configuration. The static or dynamic configuration refers to the transom draft being measured at rest or underway.

Table I: Coefficients of transom-ventilation equation

Type of Analysis	Number of Coefficients	Regression Coefficients			
		$C_1$	$C_2$	$C_3$	$C_4$
Static	2	0.1570	1.835		
	3	0.1559	1.830	0.01580	
	4	0.002472	1.862	0.2859	0.3588
Dynamic	2	0.1767	1.774		
	3	0.1795	1.786	-0.03566	
	4	0.004856	1.821	0.1990	0.3126

Table 2.2: Transom stern coefficients for transom-ventilation.[4]

Type of Analysis	Number of Coefficients	Regression Coefficients			
		$C_1$	$C_2$	$C_3$	$C_4$
Static	2	0.1135	3.025		
	3	0.09409	2.839	0.4603	
	4	0.6095	2.733	0.3468	-0.1514
Dynamic	2	0.06209	3.276		
	3	0.05598	3.179	0.2507	
	4	0.2491	3.107	0.1598	-0.1225

Table 2.3: Transom stern coefficients for hollow-length.[4]

### 2.3.4 Propeller Wake

The wake calculated is the nominal propeller wake, the wake without a propeller as the presence of the propeller will alter the flow (effective wake). The wake is calculated using the boundary layer characteristics and a velocity profile within the boundary layer. The velocity profile assumed is from that of Pretsch [11] who expanded upon a general power law distribution. The general power-law velocity distribution is,

$$\frac{u}{U} = \left( \frac{y}{\delta} \right)^n \quad (2.69)$$

where  $n$  is typically  $\frac{1}{7}$  or  $\frac{1}{9}$ .

Pretsch expanded upon the power law to include a shape factor,  $H$ .

$$\frac{u}{U} = \left[ \left( \frac{y}{\delta} \right) \frac{H-1}{H(H+1)} \right]^{\frac{H-1}{2}} \quad (2.70)$$

The shape factor,  $H$ , is the ratio of the boundary layer displacement thickness to the momentum thickness,

$$H = \frac{\delta^*}{\theta} \quad (2.71)$$

To calculate the velocity field at the propeller plane, the velocity in the boundary layer is calculated using Equation 2.70 by traversing perpendicular to the hull at each streamline from the hull to  $\delta$ , the boundary layer thickness.

$$y_{eval} = Y_{hull} + n_y \delta \frac{i}{N} \quad \text{for } i = 0 : N \quad (2.72)$$

$$z_{eval} = Z_{hull} + n_z \delta \frac{i}{N} \quad \text{for } i = 0 : N \quad (2.73)$$

where  $N$  is the number of evaluation points within the boundary layer. The evaluation points are shown in Figure 2-7.

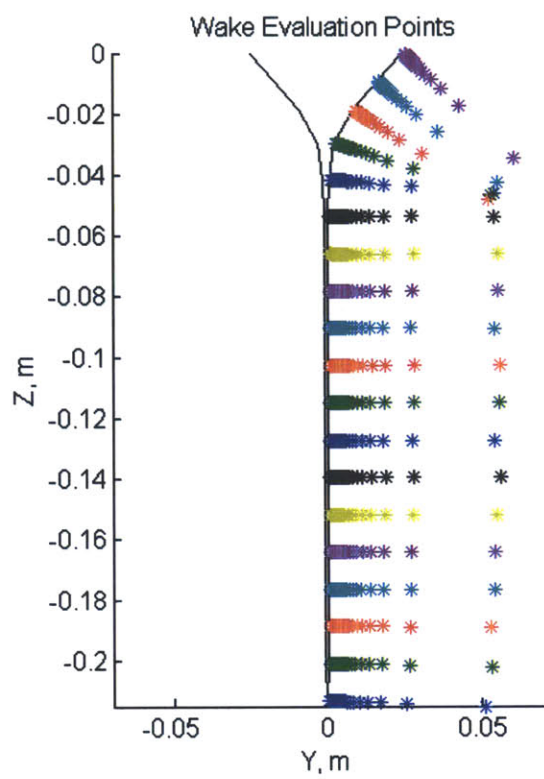


Figure 2-7: Boundary layer evaluation points used to determine propeller wake.



# Chapter 3

## Results and Discussion

### 3.1 Results

For validation, Series 60 results for  $C_B = 0.6 - 0.7$  hull forms were utilized due to the extensive test data available. Figures 3-1 through 3-3 show the body and profile plans for the Series 60 hulls used for validation. The body and profile plans are used to generate a meshed hull, shown in Figures 3-4 through 3-6. The meshed hulls do not show the actual stem and stern profiles because the meshes are rectangular with a zero offset for locations outside the actual hull surface.

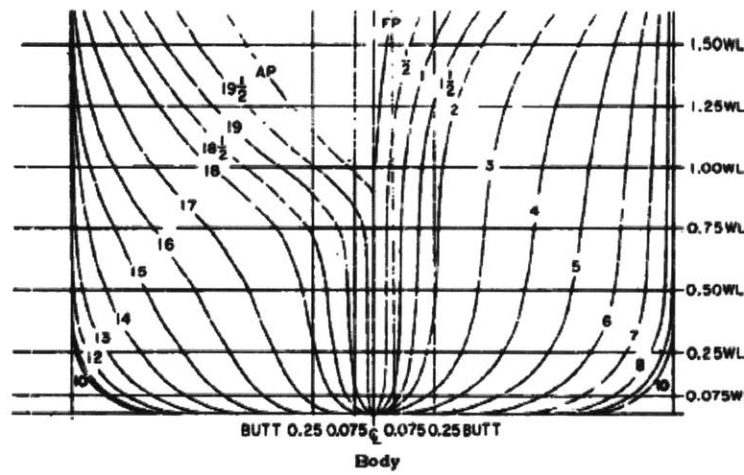
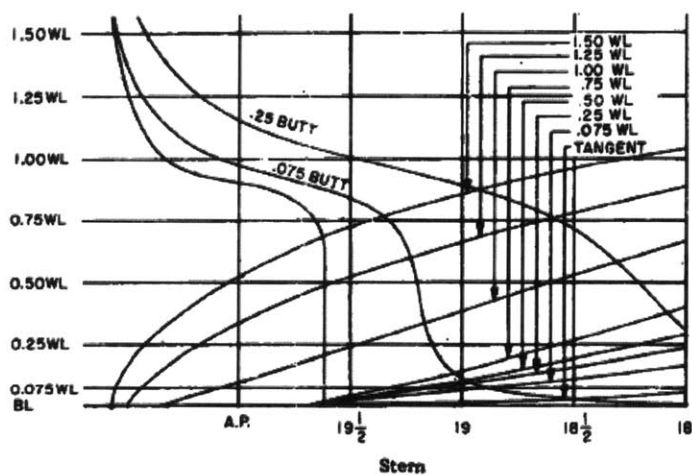
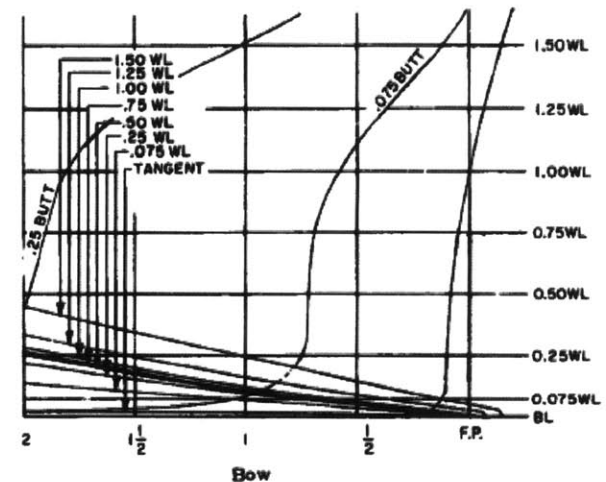


Figure 3-1: Series 60  $C_B = 0.6$  body and profile plans.[14]

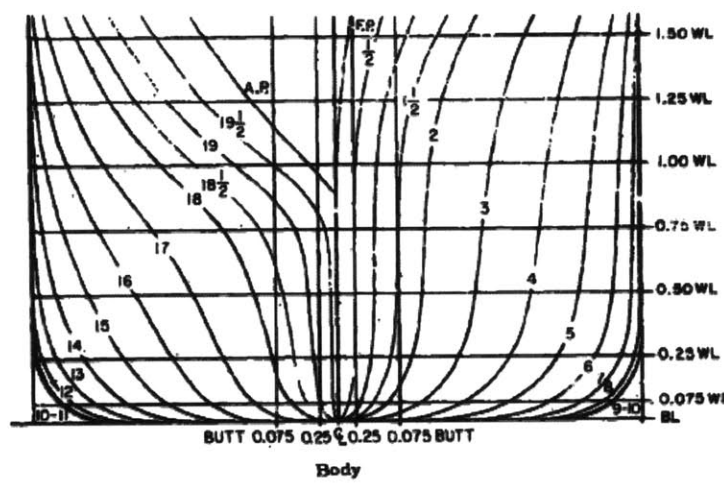
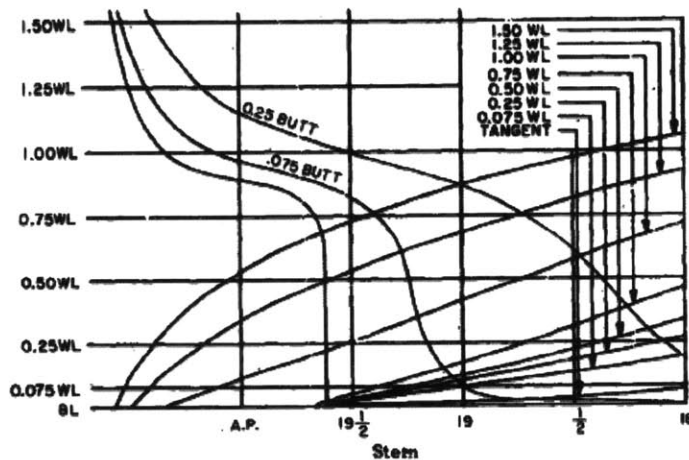
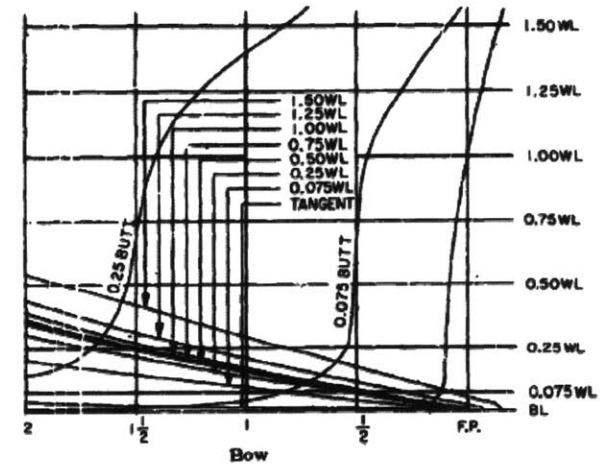


Figure 3-2: Series 60  $C_B = 0.65$  body and profile plans.[14]

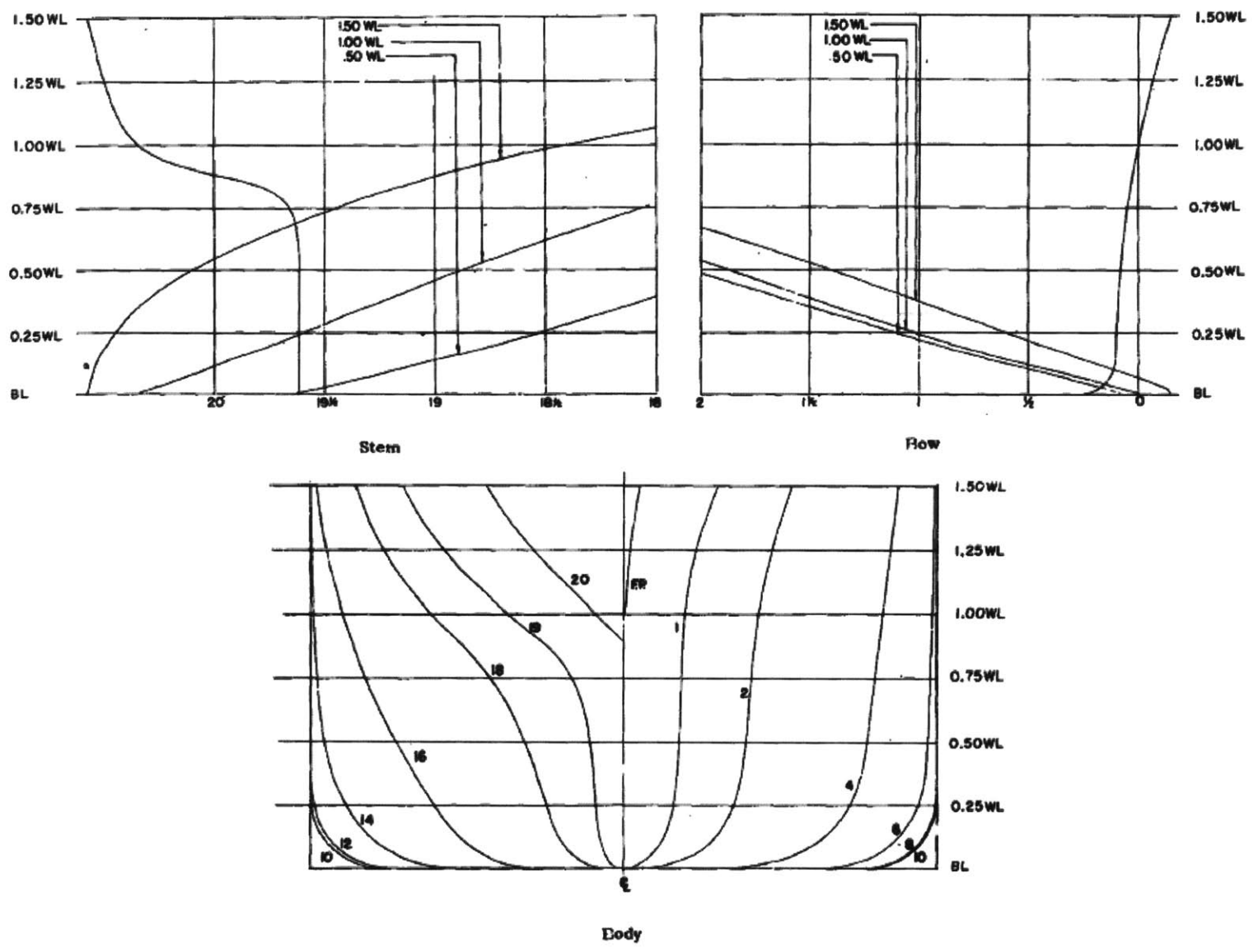


Figure 3-3: Series 60  $C_B = 0.7$  body and profile plans. [14]

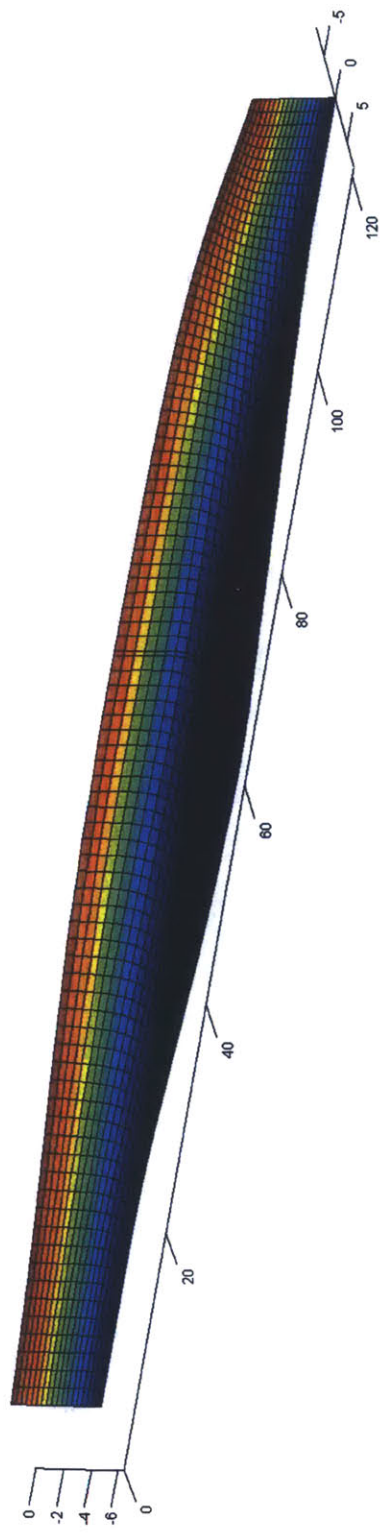


Figure 3-4: Series 60  $C_B = 0.6$  meshed hull.

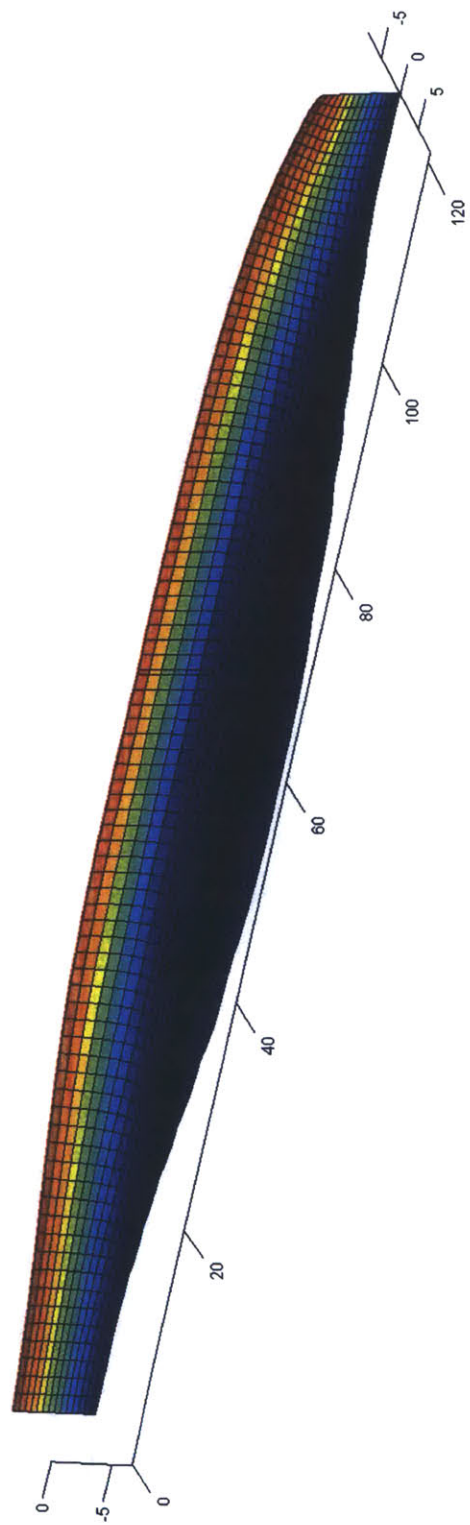


Figure 3-5: Series 60  $C_B = 0.65$  meshed hull.

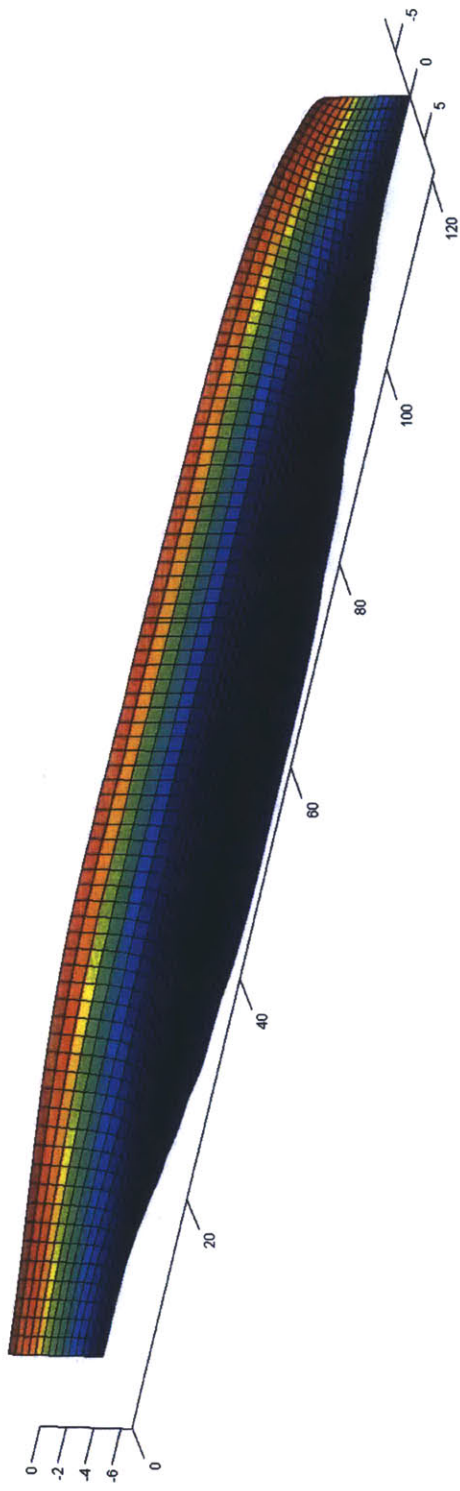


Figure 3-6: Series 60  $C_B = 0.7$  meshed hull.

The first step of the tool is to calculate the potential flow around the hull and trace the body streamlines.

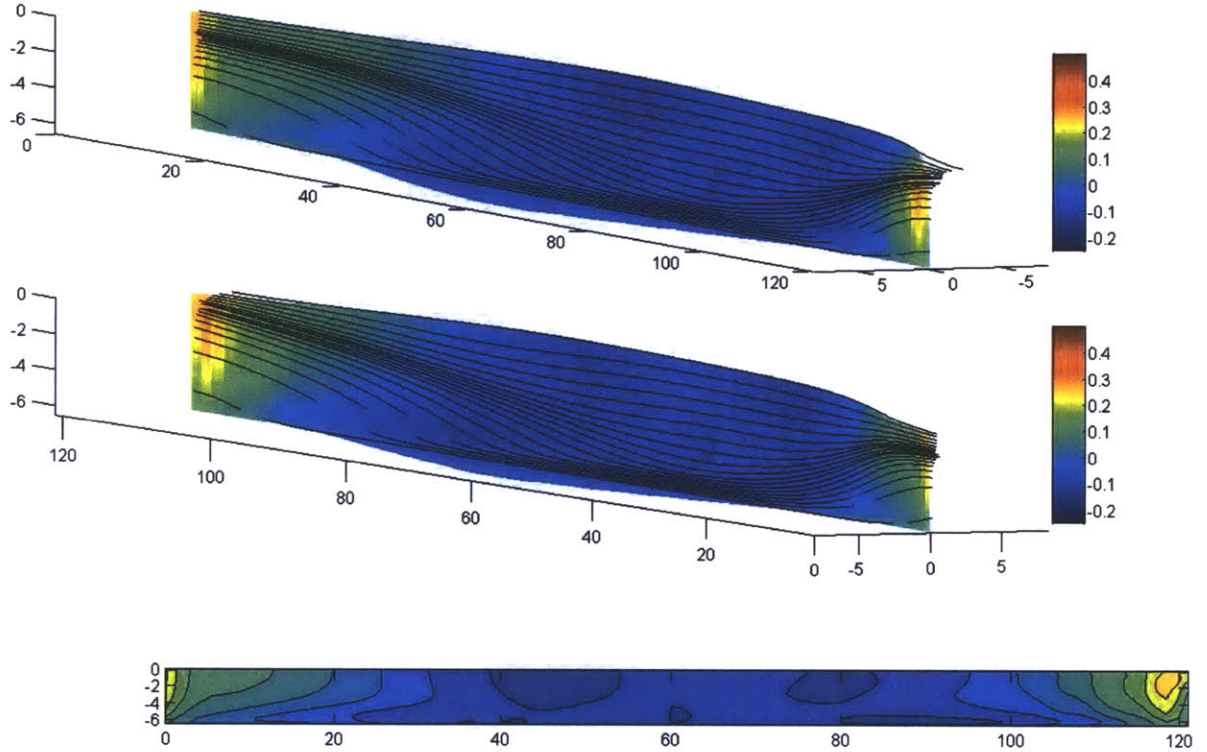


Figure 3-7: Potential flow  $C_p$  distribution and body streamlines for use with integral boundary layer calculation for  $C_B = 0.6$ . Bow to stern (top), stern to bow (middle), and side view (bottom).

Figure 3-7 is the potential flow solution for the Series 60  $C_B = 0.6$  hull depicting the pressure coefficient  $C_p$  and body streamlines. The pressure distribution is as expected with a high  $C_p$  (low velocity) at the bow and stern with a negative  $C_p$  (high velocity) midships. The change in the pressure coefficient is easily visible by examining  $C_p$  along a streamline, as shown in Figure 3-8.

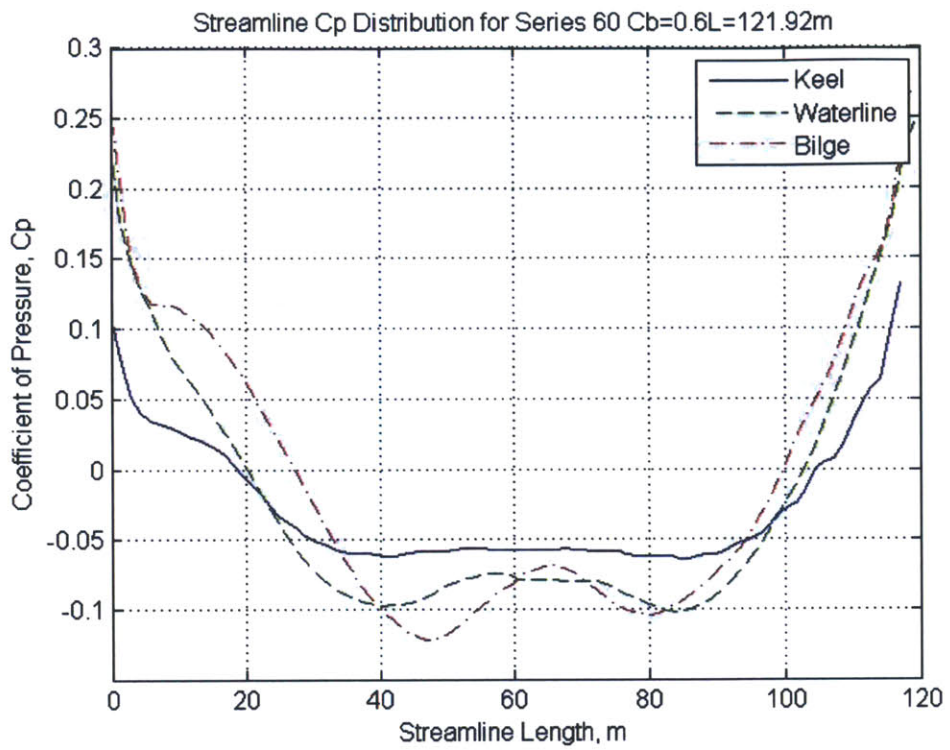


Figure 3-8: Potential flow  $C_p$  distribution along body streamlines for use with integral boundary layer calculation for  $C_B = 0.6$ .

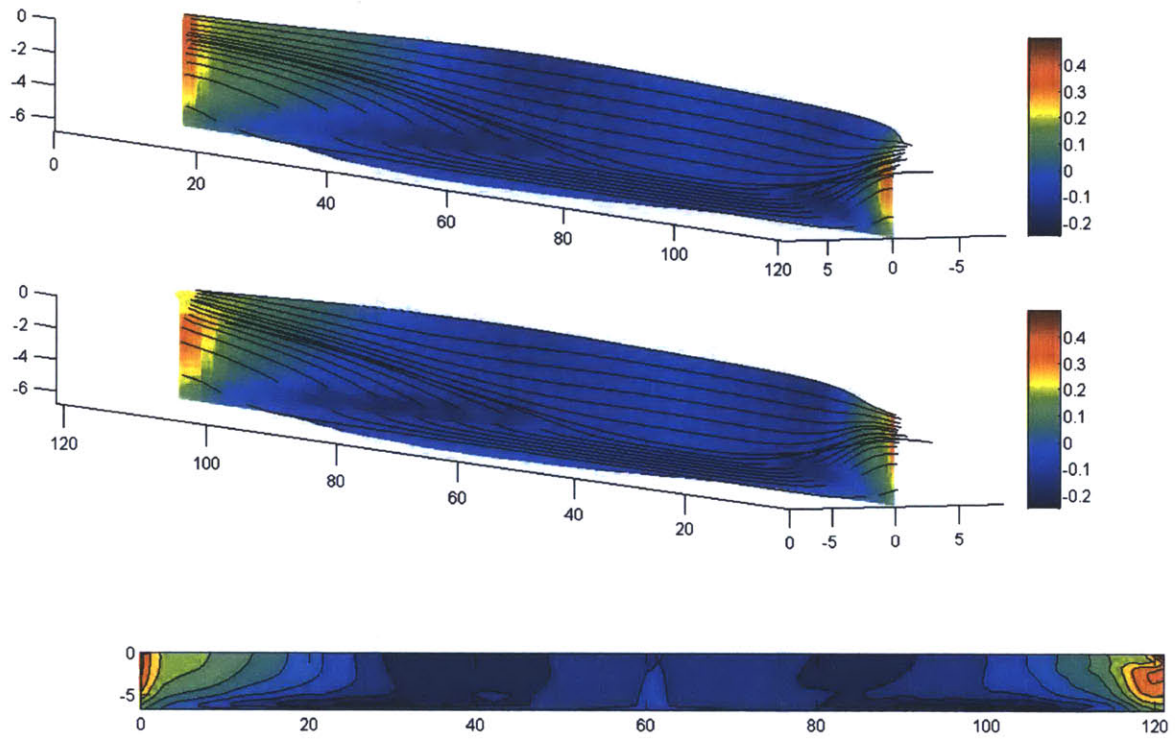


Figure 3-9: Potential flow  $C_p$  distribution and body streamlines for use with integral boundary layer calculation for  $C_B = 0.65$ . Bow to stern (top), stern to bow (middle), and side view (bottom).

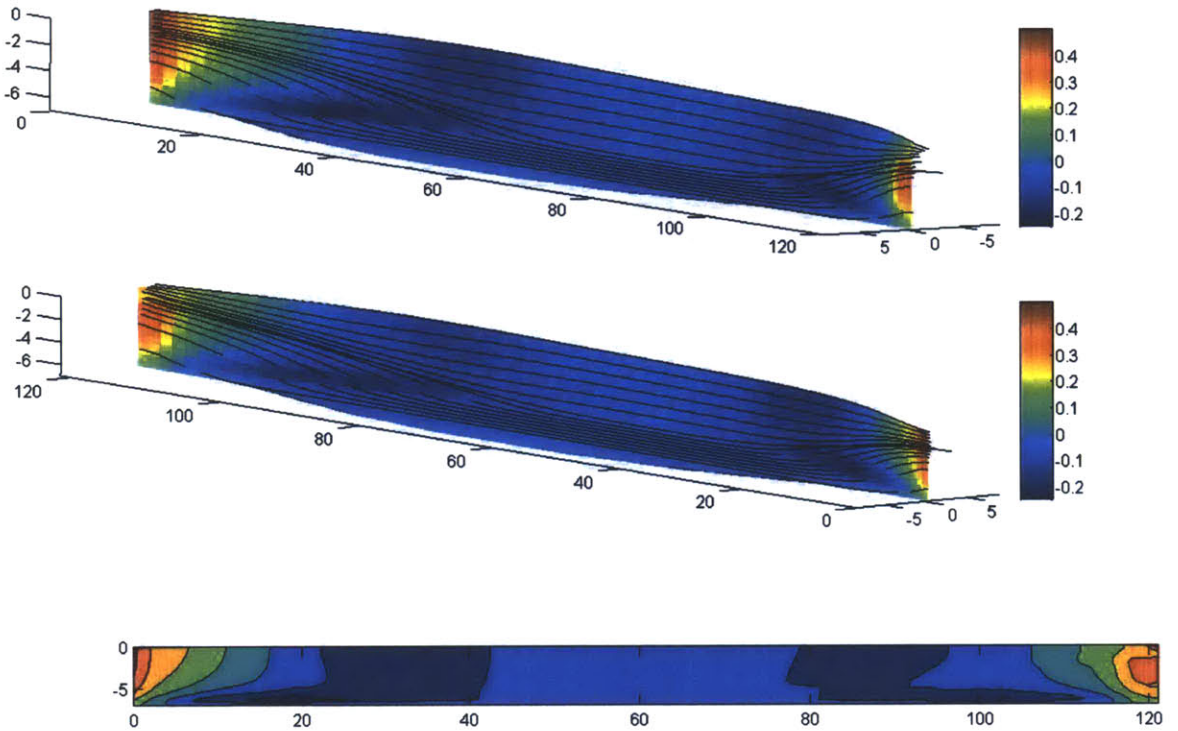


Figure 3-10: Potential flow  $C_p$  distribution and body streamlines for use with integral boundary layer calculation for  $C_B = 0.70$ . Bow to stern (top), stern to bow (middle), and side view (bottom).

Figures 3-7 through 3-10 show as the ship becomes fuller, the  $C_p$  at the bow becomes larger, acting more like a true stagnation point. The fuller ships also have a lower midship  $C_p$ , as expected.

On top of the streamlines, an integral boundary layer calculation is performed to determine the local skin friction coefficient and the boundary layer characteristics for use in calculating the viscous resistance and nominal propeller wake. To validate the frictional resistance, the predicted skin friction is compared to that of the ITTC 1957 method for a range of Froude numbers.

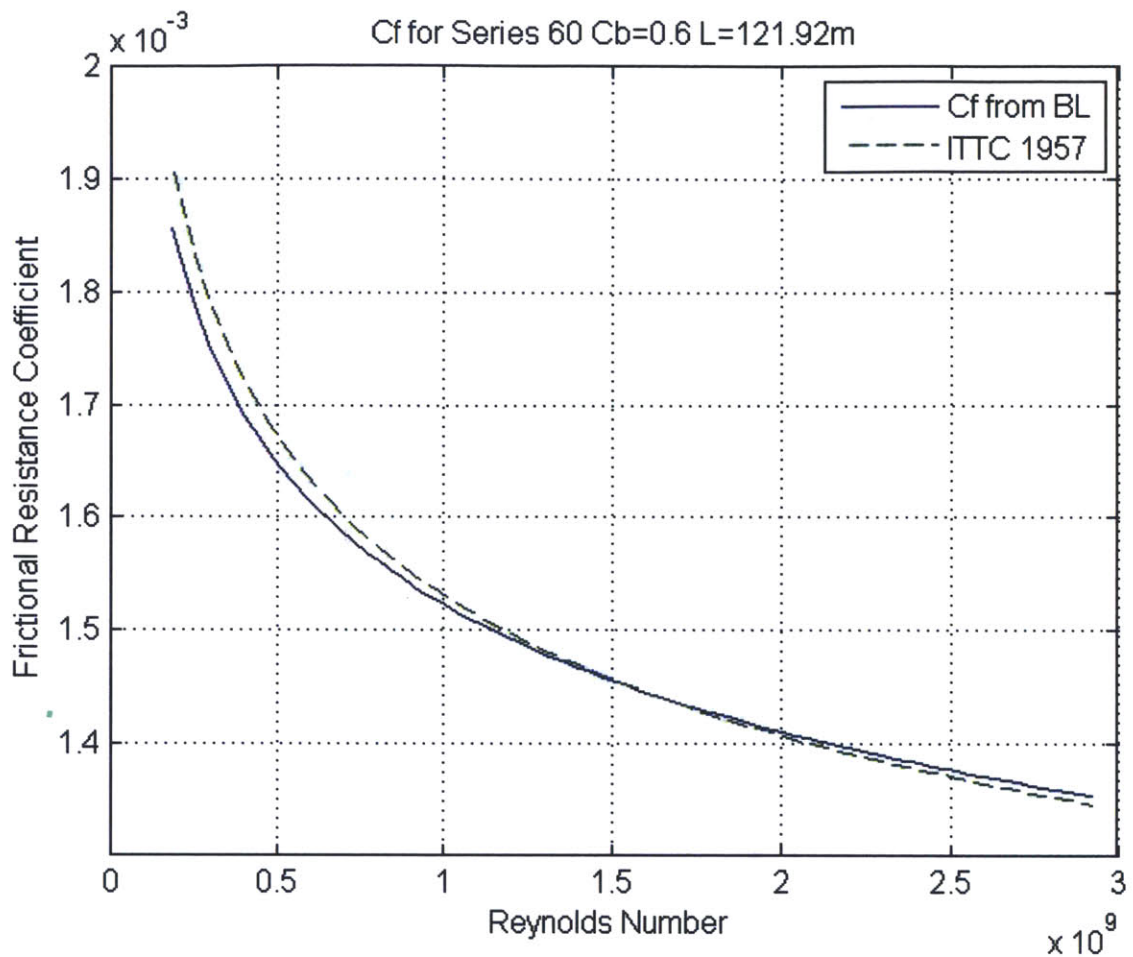


Figure 3-11: Skin friction coefficient from the integral boundary layer method compared to ITTC 1957.

Figure 3-11 shows the skin friction coefficient predicted from the integral boundary layer calculation compares well with the ITTC 1957 prediction.

The local skin friction coefficient is also plotted on the hull surface for the Series 60  $C_B = 0.60$  hull.

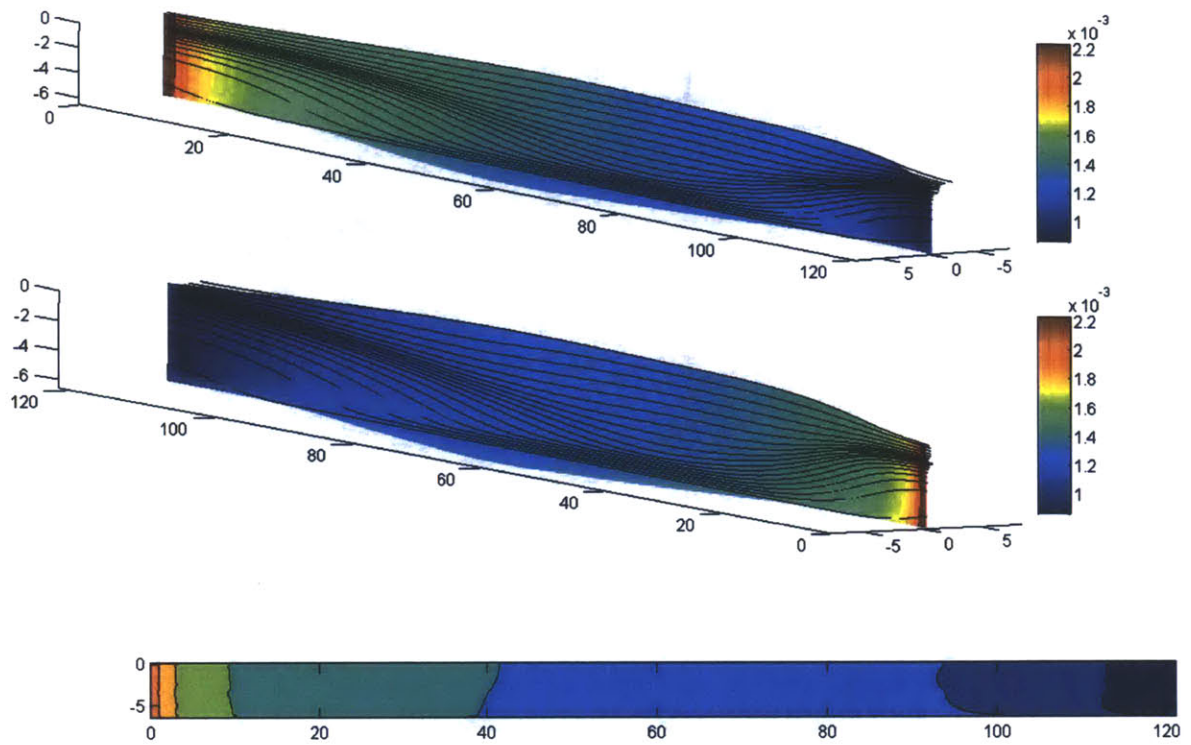


Figure 3-12: Skin friction  $C_f$  distribution from the integral boundary layer solution for  $C_B = 0.60$ .

The local skin friction results shown in Figure 3-12 are as expected with a decreasing  $C_f$  as the Reynolds number increases along the length of the ship.

The boundary layer and displacement thickness are also plotted on the hull surface.

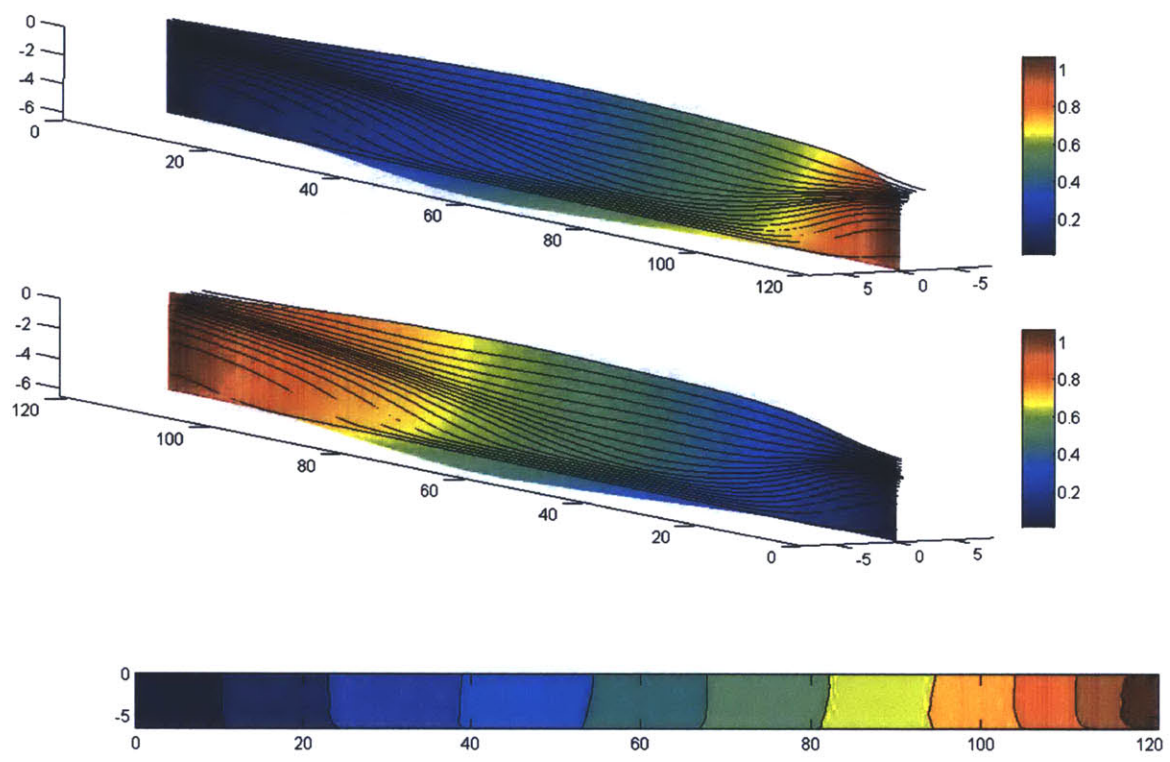


Figure 3-13: Boundary layer thickness,  $\delta$ , distribution from the integral boundary layer solution for  $C_B = 0.60$ .

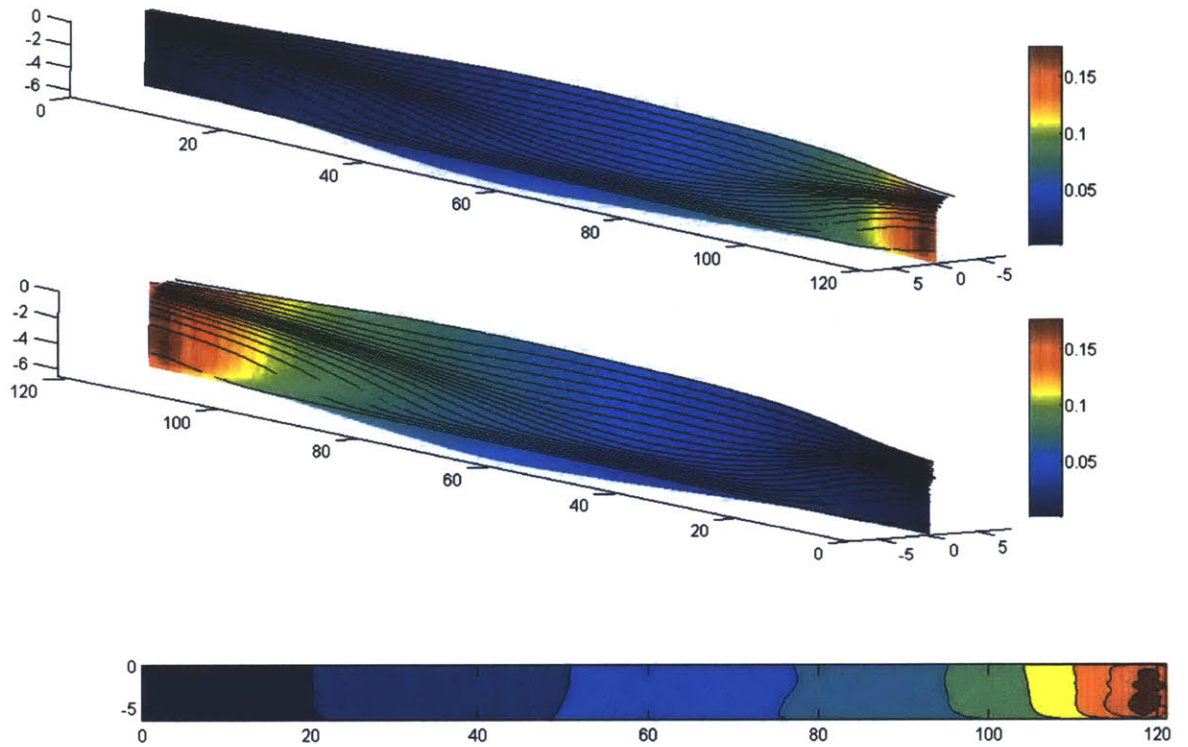


Figure 3-14: Boundary layer displacement thickness,  $\delta^*$ , distribution from the integral boundary layer solution for  $C_B = 0.60$ .

Figures 3-13 and 3-14 both show results as expected, where the boundary layer thickness,  $\delta$ , and the displacement thickness,  $\delta^*$ , increase along the length of the ship.

To compare the total resistance of the Series 60 hull at full scale to the predicted resistance, the extrapolated model tests results based on the ATTC friction line are corrected to the ITTC friction line [14]. The predicted results are adjusted because the ATTC friction line tends to underestimate the friction drag, especially at low Reynolds numbers (model tests) and therefore results in a larger residual drag coefficient and overestimate of the drag at full scale.

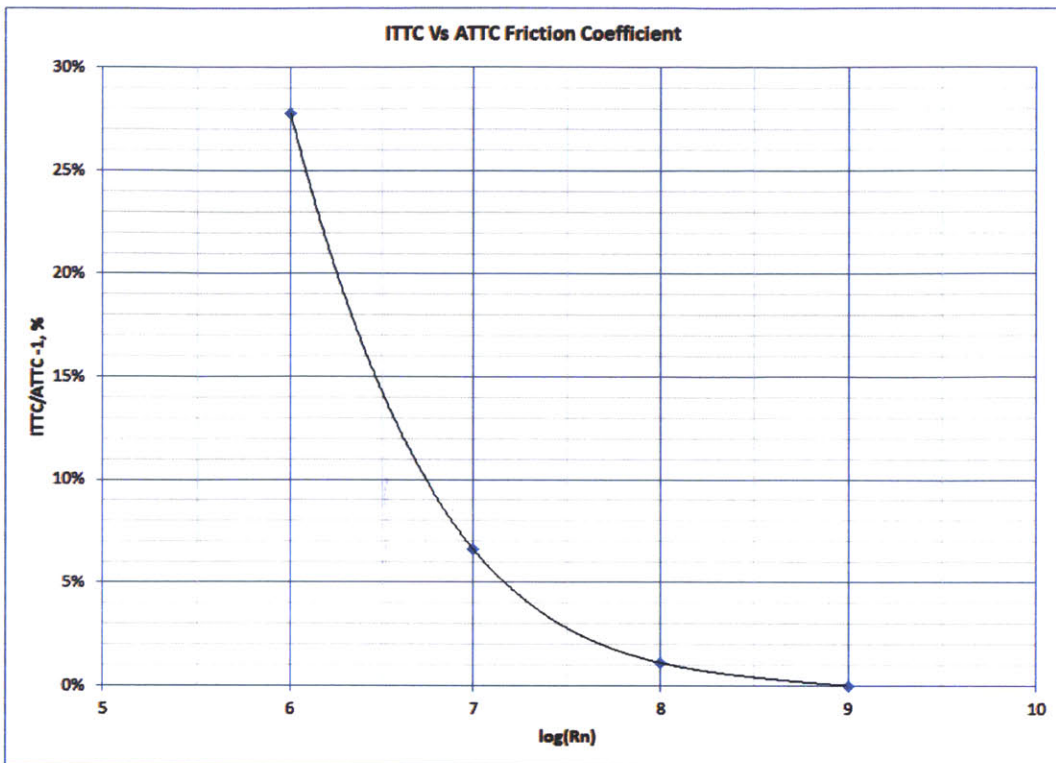


Figure 3-15: Skin friction coefficient comparison of the ATTC and ITTC friction lines.

Figure 3-15 shows in the range of the model tests  $\log_{10}(R_n) \approx 6.5$  the ITTC friction resistance is approximately 15% greater than the ATTC prediction, this means the model tests based on the ATTC friction line will have a larger residual resistance coefficient. To correct the Series 60 test data to the ITTC friction line, the ATTC friction line is used to determine the model derived residual resistance coefficient.

$$C_{r_{model}} = C_{T_{Test}} - C_{f_{ATTC}} \quad (3.1)$$

The total model scale resistance is calculated using the residual model scale drag with the ATTC friction line at model scale.

$$C_{T_{model}} = C_{f_{ATTC}} + C_{r_{model}} \quad (3.2)$$

The total resistance of the model does not change when using either the ITTC or ATTC friction lines, only the breakdown between the friction drag and residual drag changes. Therefore to determine the residual drag for the ITTC friction line, the ITTC skin friction is subtracted from the total model test resistance coefficient.

$$C_{r_{modelITTC}} = C_{T_{model}} - C_{f_{ITTC}} \quad (3.3)$$

Knowing the residual drag form the model based on the ITTC friction line, the full scale results of the model test can be extrapolated to full scale using the ITTC friction line and residual drag based on the ITTC friction line.

$$C_{T_{ITTC, Full Scale}} = C_{f_{ITTC, Full Scale}} + C_{r_{modelITTC}} \quad (3.4)$$

The form factor for each block coefficient of the Series 60 models is determined by the Watanabe formula and numerically at model scale from the separation prediction of the integral boundary layer solver.

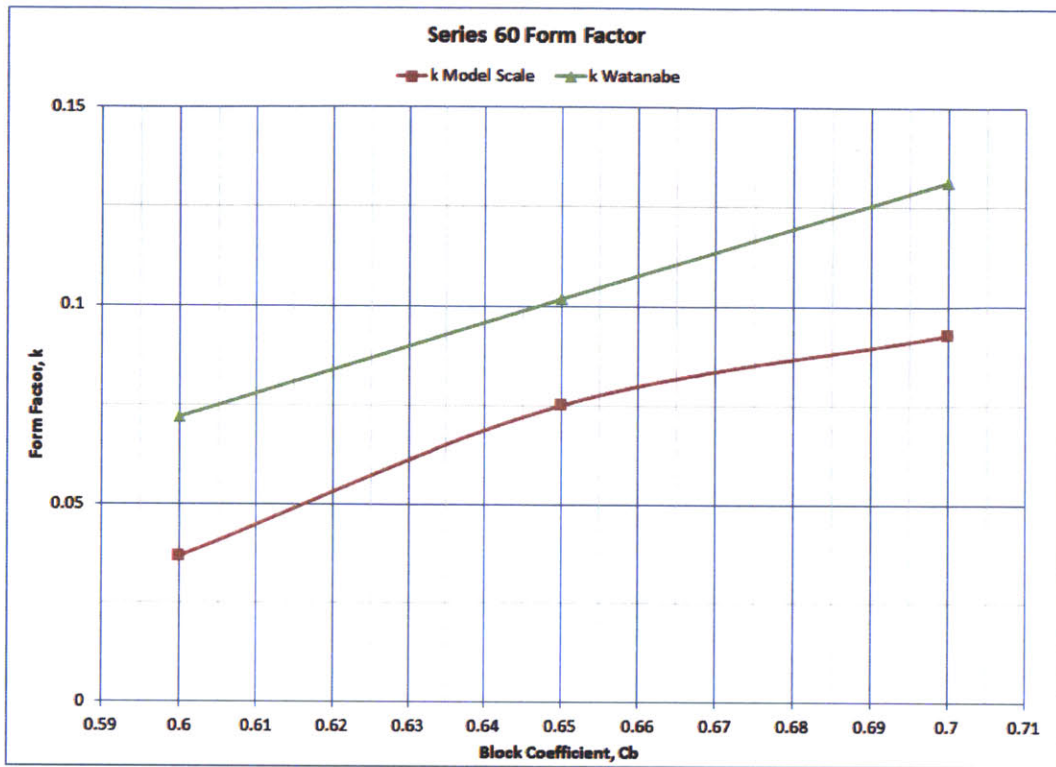


Figure 3-16: Form factor calculation comparison.

Figure 3-16 shows the numerical model scale prediction of the form factor compares well with the analytical prediction. The difference in magnitude is the numerical condition accounts for the actual geometry of the hull where the empirical method only uses coefficients of form to predict separation. The validation results are compared using both the empirical and numerical method for determining the form factor.

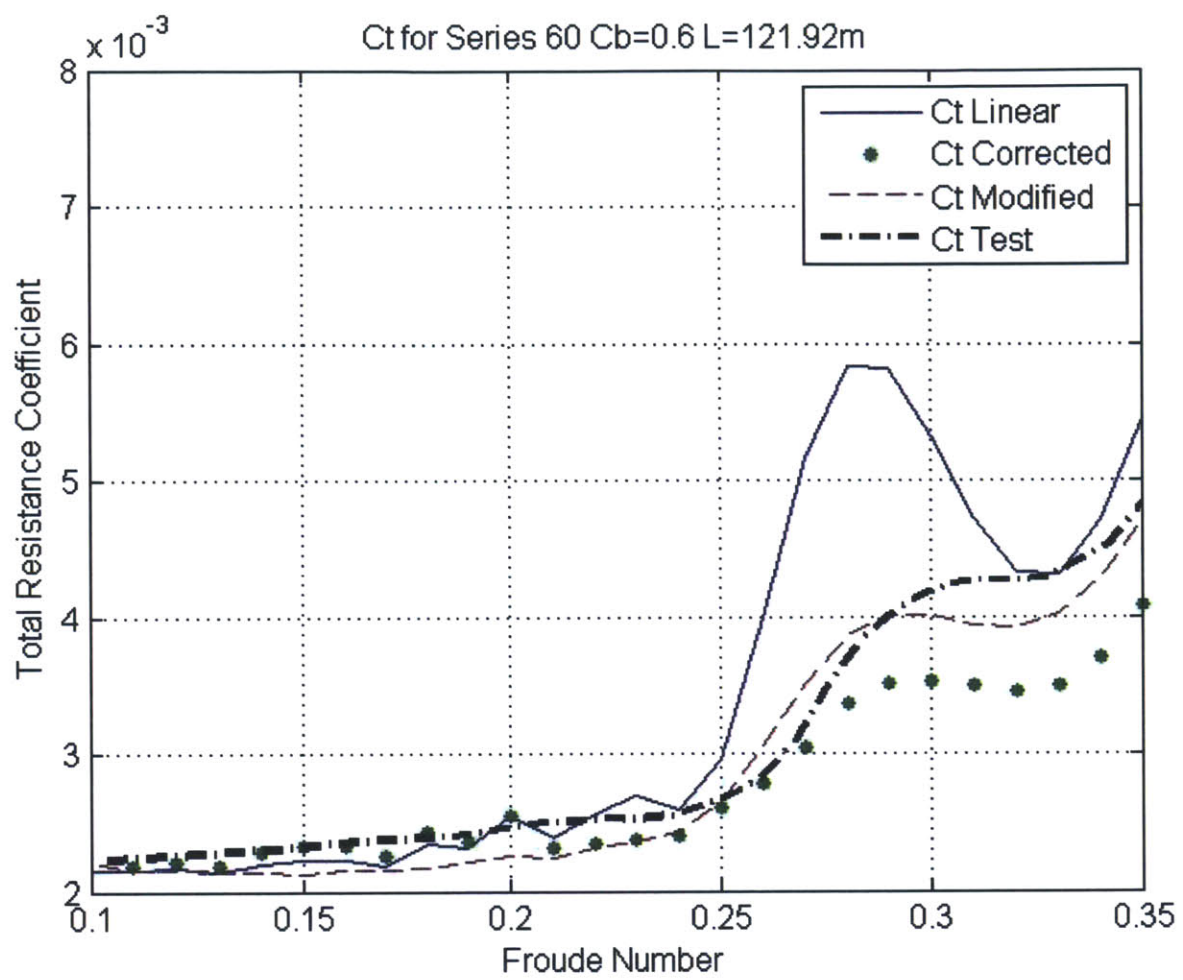


Figure 3-17: Total resistance comparison between extrapolated model test results and prediction for  $C_b = 0.6$  with numerical model scale form factor.

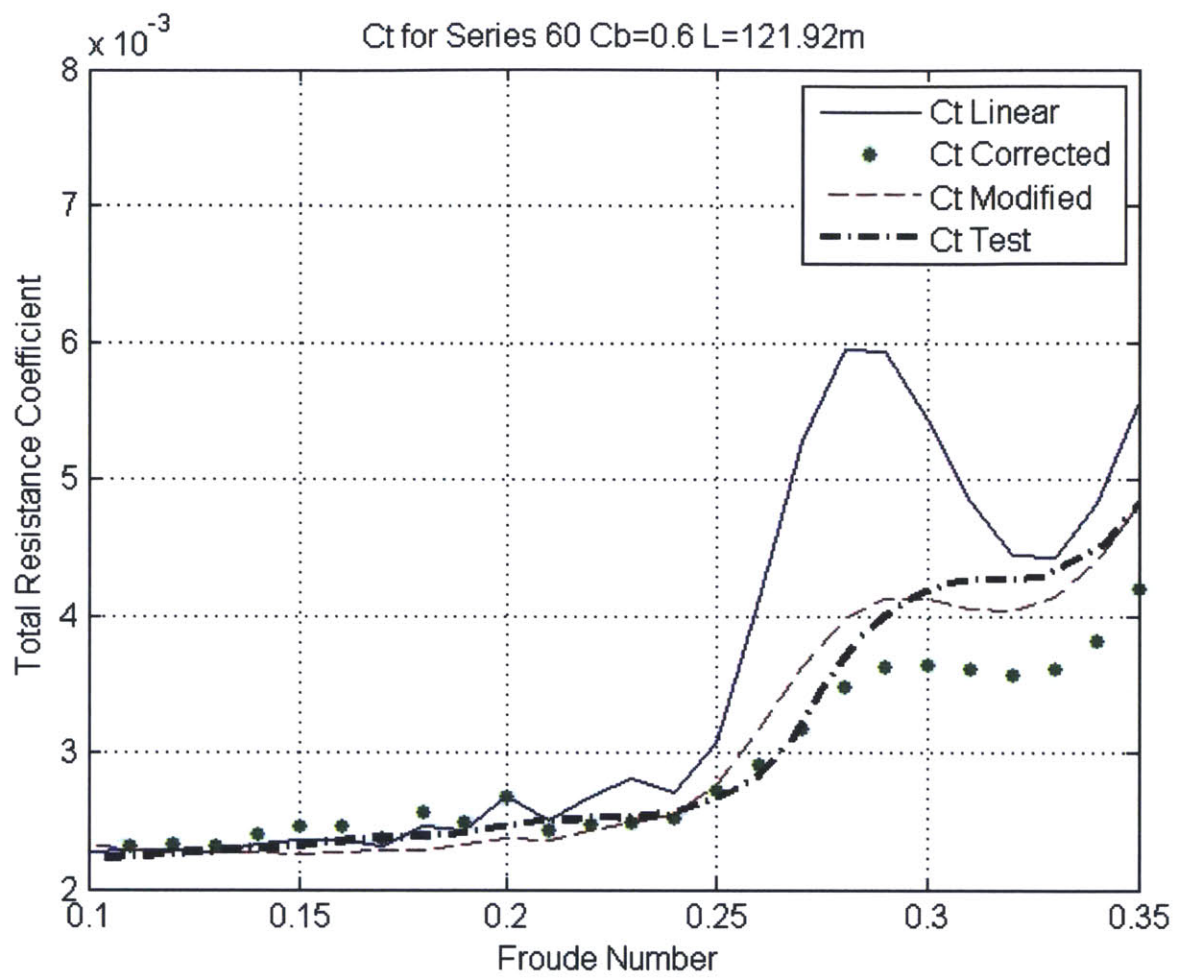


Figure 3-18: Total resistance comparison between extrapolated model test results and prediction for  $C_b = 0.6$  with empirical form factor.

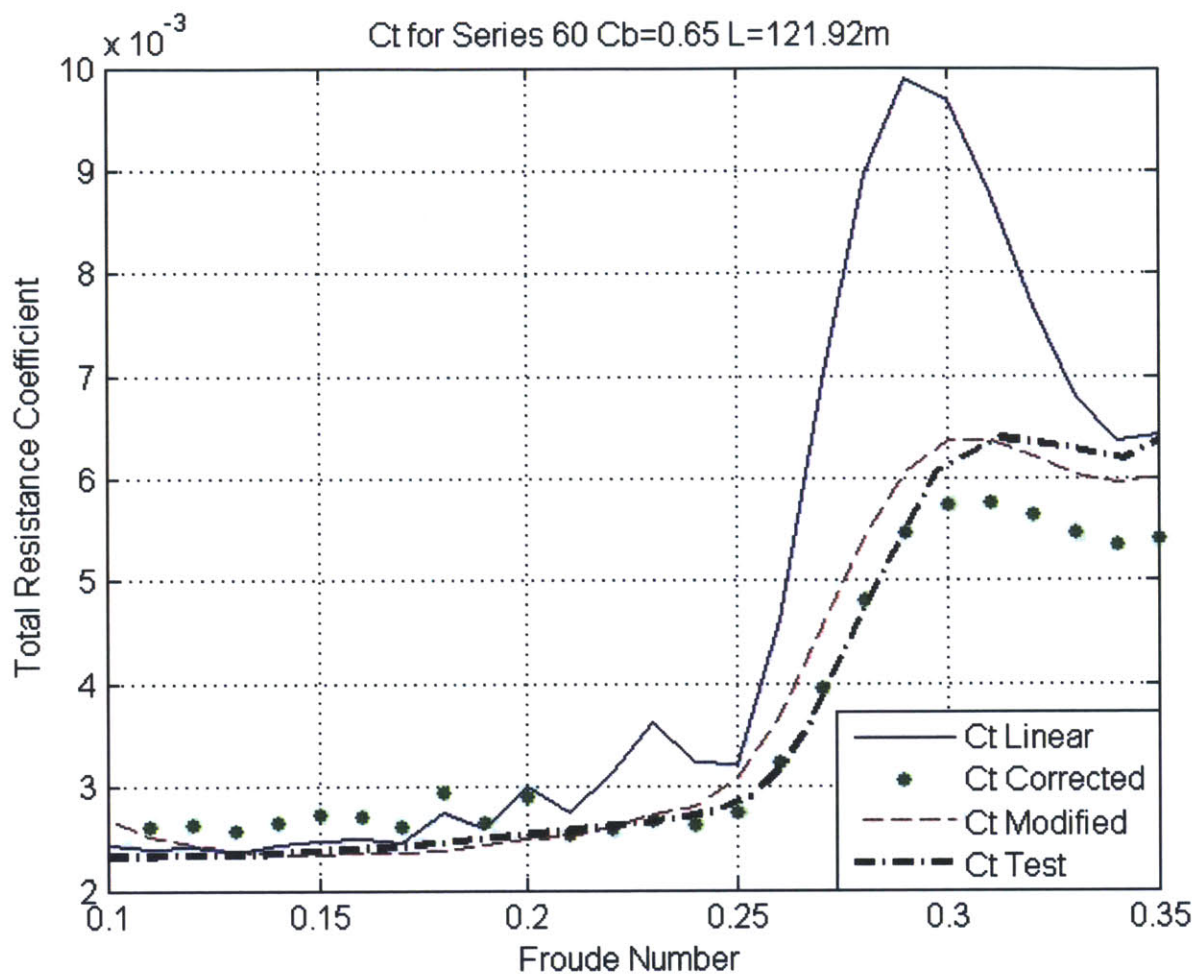


Figure 3-19: Total resistance comparison between extrapolated model test results and prediction for  $C_b = 0.65$  with numerical model scale form factor.

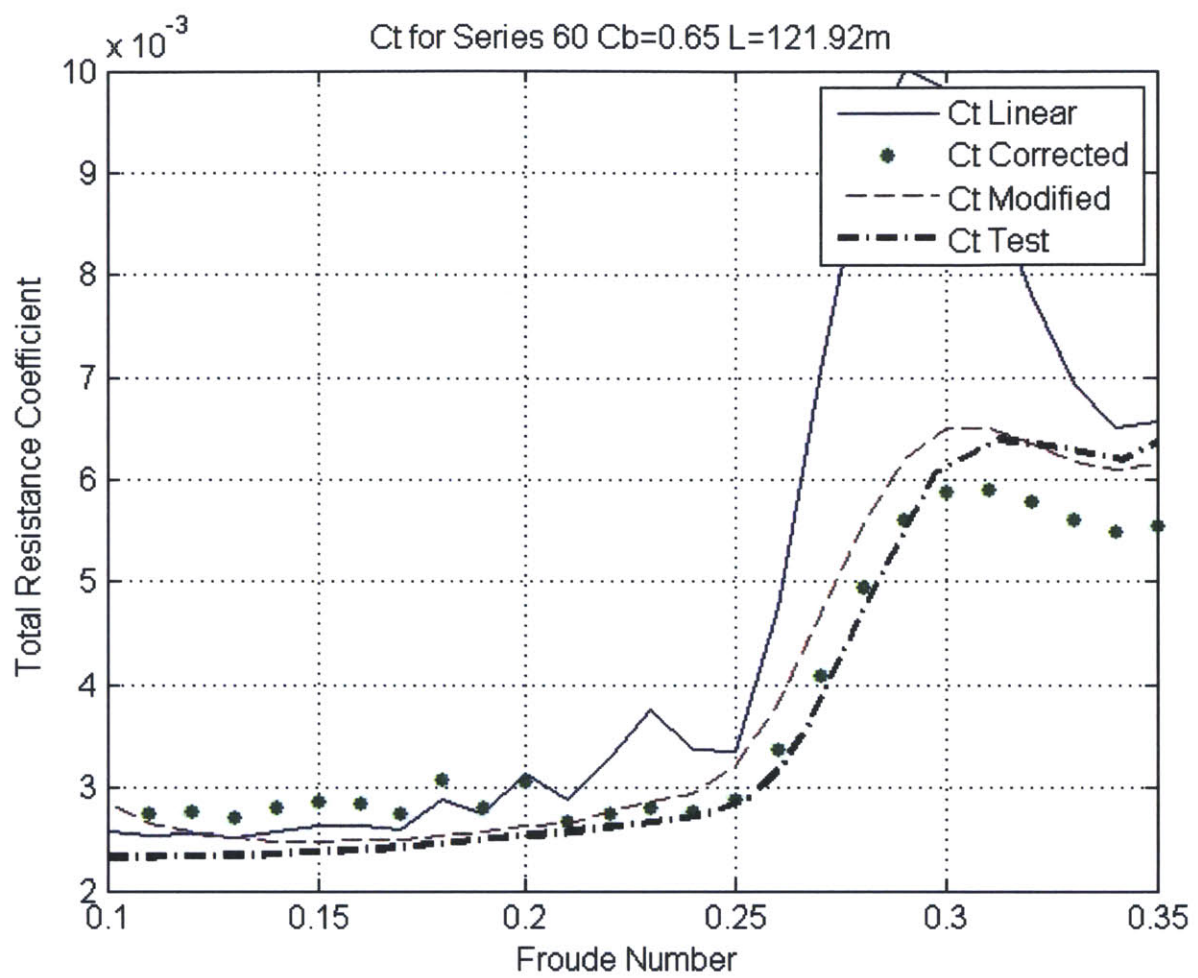


Figure 3-20: Total resistance comparison between extrapolated model test results and prediction for  $C_b = 0.65$  with empirical form factor.

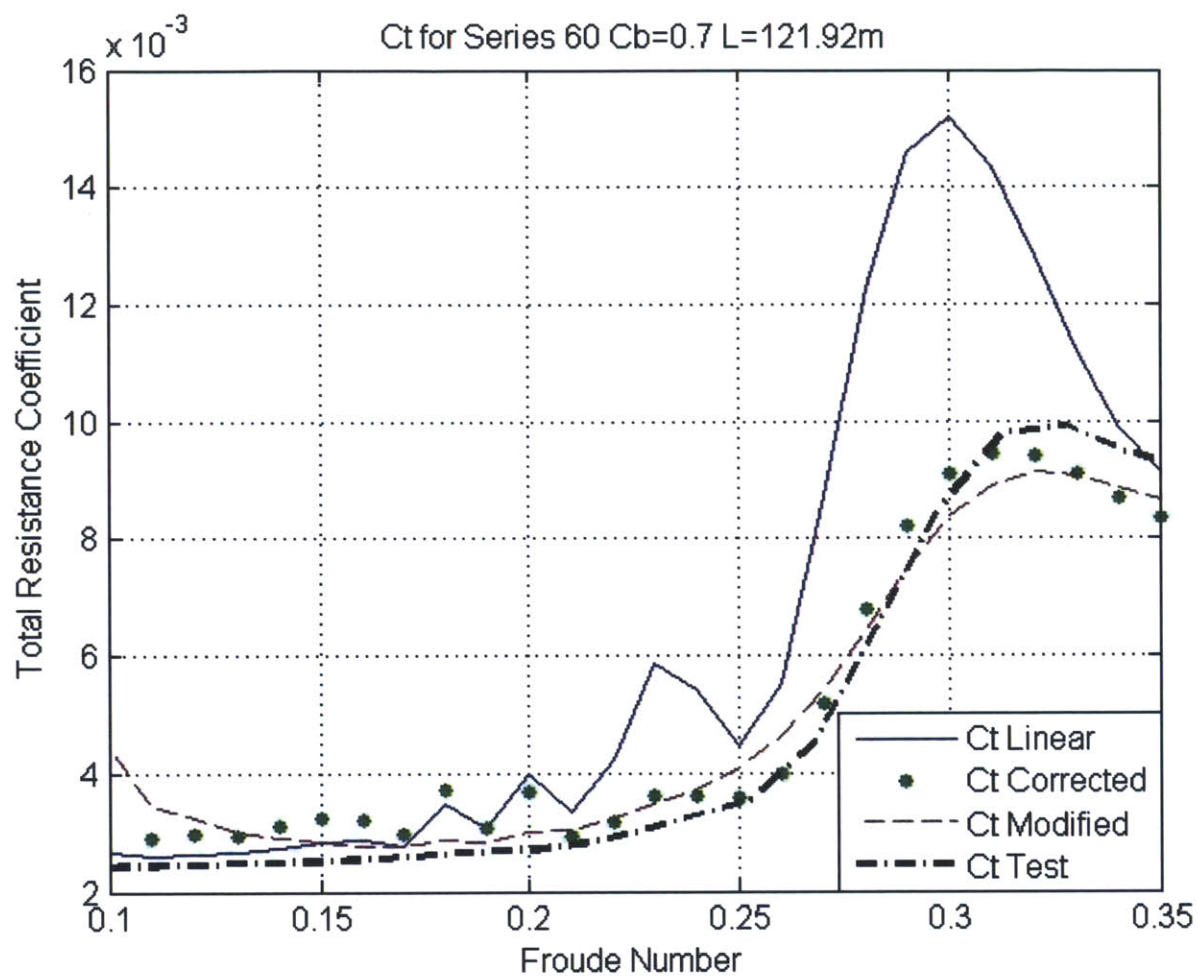


Figure 3-21: Total resistance comparison between extrapolated model test results and prediction for  $C_b = 0.70$  with numerical model scale form factor.

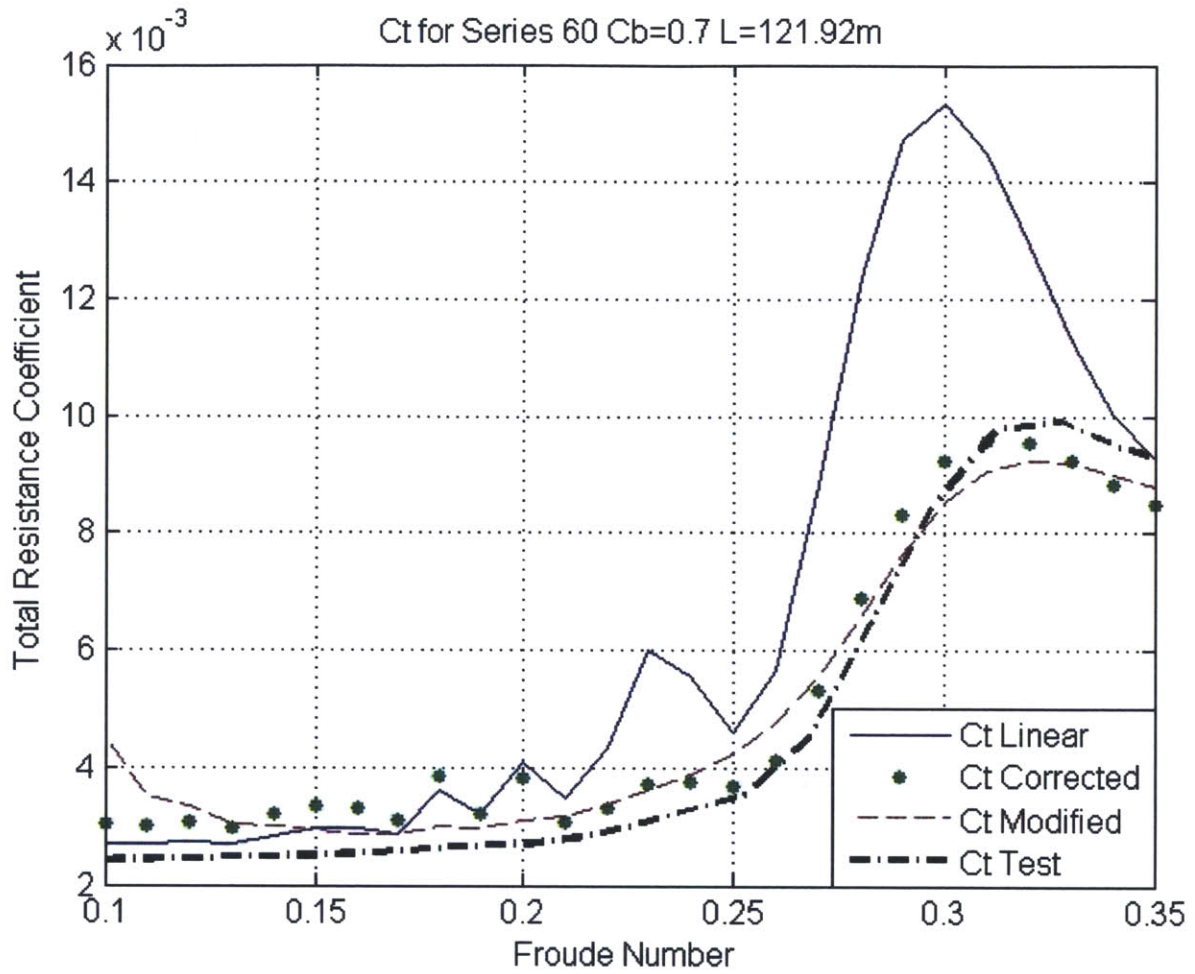


Figure 3-22: Total resistance comparison between extrapolated model test results and prediction for  $C_b = 0.70$  with empirical form factor.

Figures 3-17 through 3-22 show the results using Corrected Theory and Modified Theory for the wave drag compare well to the experimental results extrapolated to full scale. Figures 3-17 through 3-22 also show how the use of Linear Theory for the wave drag significantly overestimates the drag at higher Froude numbers and thus does not provide accurate results for a parametric study. It is also noted that the numerical predictions for the form factor at model scale improve as the fullness,  $C_B$ , of the ship increases while the empirical formula of Watanabe predicts the form factor better for slender ships.

From the integral boundary layer solution and the assumed velocity profile within the boundary layer (2.70), the flow at the propeller plane (at model scale) is visualized and compared to model test results

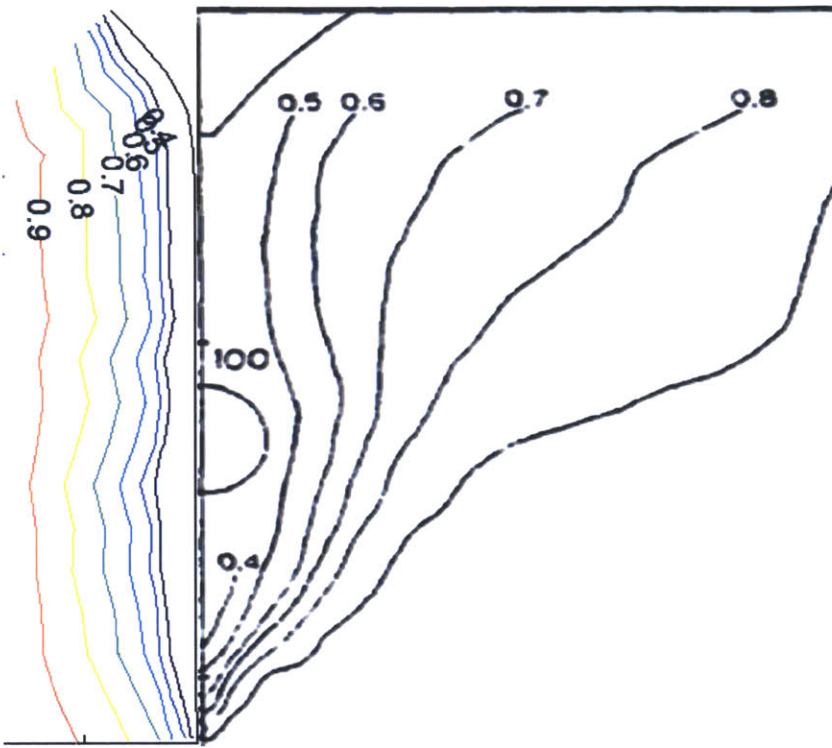


Figure 3-23: Predicted vs measured axial wake velocity contours,  $\frac{u}{U}$ .

The wake prediction is compared to the measured wake of a Series 60  $C_B = 0.6$  model test [16]. A higher fidelity estimate of the wake could be obtained by a fully coupled or weakly iterative coupled viscous/inviscid interaction (VII) method [9].

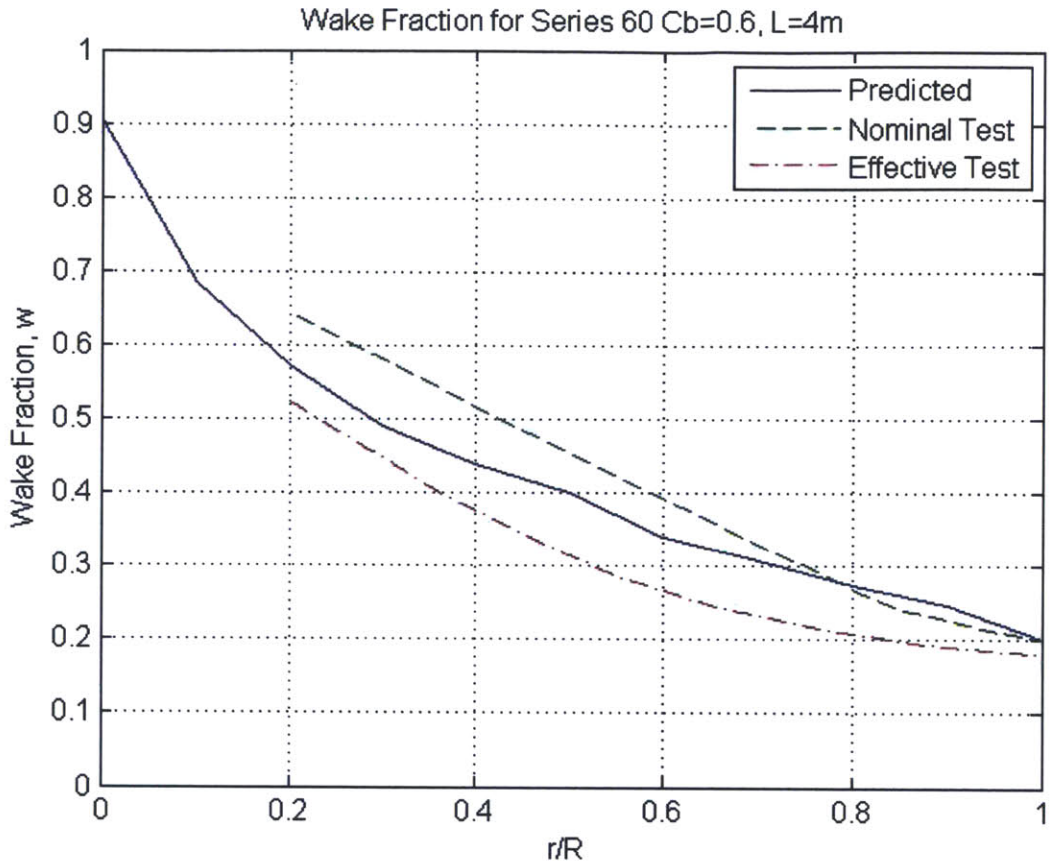


Figure 3-24: Predicted vs measured wake from model test.

Figure 3-24 shows the predicted nominal wake compares well to the measured wake and is indicatively good for preliminary design purposes. Preliminary design codes do not require a high fidelity prediction of hydrodynamic performance as the goal is to only predict the order of merit for different global variations of an initial hull form in terms of resistance and wake.

## 3.2 Conclusions

The code developed is a preliminary design tool that will allow the designer to predict the total resistance and wake characteristics of a given hull form, to be used for global optimization purposes, using propulsive efficiency as an objective function. The code

uses a 3D double body potential flow solution coupled with an integral boundary layer solver to determine the viscous drag and nominal propeller wake. The wave drag is calculated using Thin-Ship (Linear) Theory and is corrected by a series of trained panel code results [12]. The predicted results of the tool compares well to published test data of Series 60 hulls for a block coefficient range of 0.6 to 0.7. Larger block coefficients are not investigated as the Corrected and Modified Theories for wave drag are only trained to a block coefficient of 0.7. Comparing all of the validation results, the Modified Theory for wave drag best represents the test data and eliminates the additional peaks present in the Linear and Corrected Theories. To determine the form factor, the numerical method is recommended as it matches the test data well and captures the actual geometry of the hull.

Based on this work there are recommendations for tool improvement and utilization. To improve the tool the transom stern correction needs to be validated with systematic series test data. An estimate of sinkage and trim needs to be accounted for as Read [12] suggests. The integral boundary layer code could also be coupled with free surface potential flow code for determining the wave drag instead of using the double body solution and Thin-Ship Theory [7]. Another alternative is to use the double body potential flow solution with Neumann Michell theory in place of Corrected/Modified Linear Theory for the wave drag. Another tool enhancement is to validate the wake prediction of a twin screw ship as the validation was done with a single screw ship.

For future tool utilization, the code is well suited for integration into an optimization routine with a propeller. This will allow for the design a wake adapted propeller, creating an optimization objective function of total propulsive efficiency.



# Bibliography

- [1] AeroLogic. *Three-Dimensional Low Order Panel Codes*, 2004.
- [2] Giacomo Bobbiesi. Theory and numerical model of a coupled inviscid-viscid method for the analysis of partially separated hydrofoil flows. Master's thesis, University of Genoa.
- [3] Donald Coles. The law of the wake in the turbulent boundary layer. Technical report, California Institute of Technology, 1956.
- [4] Lawrence J. Doctors. A numerical study of the resistance of transom-stern mono-hulls. Technical Report Ship Technology Research Vol.54-20007, The University of New South Wales, 2007.
- [5] L. Lazaukas E.O. Tuck and D.C. Scullen. Sea wave pattern evaluation: Part 1 report: Primary code and test results (surface vessels). Technical report, The University of Adelaide, 1999.
- [6] Chi Yang Francis Noblesse, Fuxin Huang. The neumann-michell theory of ship waves. Technical Report Journal of Engineering Mathematics; Vol. 79, David Taylor Model Basin and George Mason University, 2009.
- [7] Stefano Brizzolara Iacopo Biliotti. Automatic parametric hull form optimization of fast naval vessels. Technical Report 11th International Conference of Fast Sea Transportation, Department of Naval Architecture, Marine Engineering, and Electrical Engineering, University of Genoa, Italy, 2011.
- [8] Lars Larsson and Hoyte C. Raven. *The Principle of Naval Architecture Series: Ship Resistance and Flow*. The Society of Naval Architects and Marine Engineers, 2010.
- [9] William Milewski. *Three-dimensional viscous flow computations using the integral boundary layer equations simultaneously coupled with a low order panel method*. PhD thesis, Massachusetts Institute of Technology, 1997.
- [10] J.G Nash, J.F.;Hicks. An integral method including the effect of upstream history on the turbulent shear stress, computation of turbulent boundary layers. Technical report, Stanford University Press, 1969.

- [11] J Pretsch. Theoretical solution of profile drag. Technical report, NACA TM 1009, 1942.
- [12] Douglas Read. *A Drag Estimate for Concept-Stage Ship Design Optimization*. PhD thesis, The University of Maine, 2009.
- [13] Gary Saaris. *A5021 User's Manual-PAN AIR Technology Program for Solving Problems of Potential Flow about Arbitrary Configurations*. Boeing, 1992.
- [14] F.H. Todd. Series 60 methodical experiments with modeles of single-screw merchant ships. Technical Report Report 1712, David Taylor Model Basin, 1963.
- [15] Petros Voxakis. Ship hull resistance calculations using cfd methods. Master's thesis, Massachusetts Institute of Technology, 2012.
- [16] I. Tanaka Y. Toda, F. Stern and V.C. Patel. Mean-flow measurements in the boundary layer and wake of a series 60  $c_B = 0.6$  model with and without propeller. Technical Report IIHR Report 326, Iowa Institute of Hydraulic Research, The University of Iowa, 1988.